Spatial and Geographic Analysis of European and Southwest North American Dust Storms

by

Joshua R. White

A Dissertation Presented in Partial Fulfillment
of the Requirements for the Degree
Doctor of Philosophy

Approved March 2024 by the
Graduate Supervisory Committee:

Randall S. Cerveny, Chair
Robert C. Balling Jr.
Anthony Brazel

ARIZONA STATE UNIVERSITY

May 2024

ABSTRACT

Dust storms have far-reaching human and economic impacts; spreading disease, raspatory and cardiovascular disruption, destruction of property and crops, and death. Understanding of this phenomenon is can help with operational and academic endeavors and alleviate some of these impacts. To accomplish this goal, this dissertation poses a central question: Do dust storms have discreet geographic and temporal characteristics that can aid academic and operational analysis of these storms? To answer this question three case studies were undertaken. The first study constructed an archive of 549 dust rain events across Europe to determine a seasonal pattern. It was discovered that the largest number of events occurred in the Spring season (MAM). Then three individual events across Europe were examined to highlight the synoptic events that control these dust rains. Each event can be closely tied to the movement of the migratory Rossby waves and linked to Saharan dust from North Africa. The second study was a construction of Central Sonoran Desert dust storms from 2009 to 2022 tied to the NAM. HYSPLIT back-trajectories linked the strongest events to source regions mainly from the Southwest along the Gila River from the Gulf of California. As the storms weaken in intensity they drift to the South and Southeast traveling along the Santa Cruz River and its tributaries. The third study was a case study of three large events in the Central Sonoran Desert along the Gila River. This study examines the effects of the local topography, specifically the stand-alone mountain complexes that can block or funnel dust as it moves through the Gila River Valley. In each instance the South Mountain Complex and the Sierra Estrella served as a dust shield containing the highest dust concentrations to the south side of the Gila River Valley. This dissertation has analyzed

several of the different elements of dust storms. These elements include the synoptic patterns that drive dust storms, the source regions of dust storms, and the ground level topography that can control their movement. Fundamentally, these findings can enhance our academic understanding of dust storms as well as our operational ability to forecast.

DEDICATION

I dedicate this dissertation to my family and friends. My mother Glenda, who nurtured me. My father Darrell, who taught me to be a man. Your unwavering support and belief in me made this possible. My brother and sister Darrell II and Shelley, you both inspired the scientist in me to explore. My best friend Dr. Jacob Hiscox, you helped me find my path. May the lord bless and keep you all, you have my eternal thanks.

ACKNOWLEDGMENTS

There are a few individuals who made my success possible and I would like to thank those people here. My chair, Dr. Randall S. Cerveny, you have been a wellspring of support, patience, wisdom, and enthusiasm. I am forever grateful for your guidance and faith in me. My committee members, Dr. Robert C. Balling Jr., who helped me acquire the skills necessary to complete this project, and Dr. Anthony Brazel, who's own work laid the foundations which I build upon. You were both instrumental to my work, thank you both so much for your support. A special thank you to Dr. Elizabeth Wentz Vice Provost & Dean, Graduate College and Vice Provost/Dean & Professor to the School of Geographical Sciences and Urban Planning, you gave me the chance I needed to complete this work. I am so grateful for your aid, and belief in me.

TABLE OF CONTENTS

CHAPTER Page

CHAPTER Page

LIST OF TABLES

TABLE Page

LIST OF FIGURES

FIGURE Page

CHAPTER 1

1.1 Introduction

Dust storms are a global phenomenon with varied and far-reaching consequences. With reduced visibility and high winds accidents are a common occurrence during any dust storm event. According to a recent study, in the United States alone, dust storms have been responsible for 232 deaths between 2007-2017 (Tong et al. 2023). Most of those deaths occurred in the Southwest region of the country. Besides the immediate risk of death caused by dust storms, there are other human health impacts to consider. Respiratory and cardiovascular issues arise when small particulates are inhaled, as well as the transfer of a variety of microorganisms that cause disease such as: meningococcal meningitis, coccidioidomycosis, conjunctivitis, valley fever, and measles (Goodie 2020).

Beyond the human health risks there are also wide-reaching economic impacts caused by dust storm activity. During that same period of 2007-2017 previously referenced the storm event database estimates 7.3 million dollars in property damage and 5.8 million dollars in crop damage caused by dust storms (NCEI 2024). The crop destruction and wind erosion caused by dust storms can have more long-lasting side-effects as well. According to Shepard (2016), the estimated off-site cost of the wind erosion and decreased soil productivity for the state of New Mexico alone is 466 million dollars a year. These costs are not limited to the United States, from 2010-2013 the economic losses for China croplands were estimated at 964 million dollars (Shepard 2016). Dust storms an important and consequential element of our environment and need to be better understood.

Dust storms an important and consequential element of our environment and need to be better understood. As a result, this study will examine the movement of dust storms and controls on that movement. To accomplish this, I have undertaken three separate case studies examining different elements of dust storm movement through time and space.

1.2 Problem Statement

Previous studies on dust storms have examined the elements that define a storm and control their spread and duration. Dust storms have been defined by the level of visibility (Brazel and Nickling 1986, Nickling and Brazel 1984, Goudie 1983). The duration and spread of dust events (Nickling and Brazel 1984, Rivera Rivera et al. 2010), as well as the chemical composition of the dust itself have also been used to define them (Rogora, et al. 2004, Reynolds et al. 2006).

Beyond defining the elements, there have been studies on dust storms that have examined different tools and methods to track and identify them. Tools like: TOMS Aerosol Index, HYSPLIT READY, NCEP/ NCAR and NARR Reanalysis, and IDW interpolation. A study using the TOMS AI was able to identify decreased visibility during the Harmattan season due to dust storm activity across sub-Saharan West Africa (Ogunjobi et al. 2012). A study using NCEP/NCAR Reanalysis was used to identify the synoptic patterns linked with dust storm activity in the Middle-East and North African region, including Shamal dust storm which are linked to high pressure systems establishing over the region (Hamidi et al. 2013) HYSPIT back trajectories of dust storm events have been used numerous timed to identify the source region, for instance source regions over North Africa and the Arabian Peninsula were identified for dust storms in Kuwait (Yassin et al.

2018). Lastly, studies using IDW interpolation have been used to map PM 2.5 and PM10 sensor data over large urban areas, for instance a study in 2016 IDW interpolation was used to map the spread of dust events over Beer-Sheva in southern Israel (Krasnov et al. 2016)

To help further understand dust storms and their movement I use these tools to answer this central question:

a) *Do dust storms have discreet geographic and temporal characteristics that can aid academic and operational analysis of these storms?*

Given that central question I can break this study into three separate themes:

b) *Is there a definable seasonal component to European dust "blood" rain events?*
c) *Is there a specific origin source for monsoon convective dust storms in the central Sonoran Desert region?*
d) *What topographic elements effect the movement of monsoon convective dust storm in the central Sonoran Desert region?*

To answer these three questions, I have conducted three separate studies. The first study is *Seasonality in European Red Dust/ "Blood" Rain Events.* It was published in the *Bulletin of the American Meteorological Society* in April 2012. The second study is *Trajectory Analysis of Central Sonoran Desert Dust Storms.* It was published in the *Journal of Arid Environments* in December 2023. The third study is *Topographic Dust Shielding and Funneling: North American Monsoon Case Studies for the Sonoran Desert, Central Arizona, USA.* It is submitted for publication in the *Journal of Arid Environments*.

1.3 Dissertation Framework

Given the central question to this dissertation regarding dust storm movement, I propose to explore different temporal and spatial elements of dust storms in order to answer that question. I will begin with long range dust transport from the Sahara Desert associated with colored rain phenomenon across Europe. Secondly, I examine dust transport over the Sonoran Desert during the NAM into the Gila River Valley and identify source regions for those events. Thirdly, I examine the movement of a few of the largest events in the Sonoran Desert and how the local topography effects their movement through the Gila River Valley.

1.3.1 Case Study 1

Chapter 2 contains the research paper that focuses on the first subordinate research question regarding long range transport of Saharan Dust across Europe. This study involves the construction of a comprehensive dust rain event archive of 549 events using published papers, satellite imagery, limited media accounts of the phenomenon. Those events where broken into seasons based on three-month grouping: Winter (DJF), Spring (MAM), Summer (JJA), and Autumn (SON). After identifying the seasonal trends three case examples were explored to show the transport and the synoptic conditions driving the events. For the case examples HYSPLIT back-trajectories, NCEP/NCAR Reanalysis of 700 and 500 hPa height contours, 700 hPa relative humidity by percent, and the TOMS AI values were used to show the dust movement across Europe. This study has a version that was published, titled as: Seasonality in European red dust/ “blood” rain events. It was published in the *Bulletin of the American Meteorological Society* on April 1, 2012

doi: 10.1175/BAMS-D-11-00142. The co-authors on this paper are Randall S. Cerveny and Robert C. Balling, Jr.

1.3.2 Case Study 2

Chapter 3 contains the research paper that focuses on the second of my subordinate research questions involving NAM convective dust storms that form in the central Sonoran Desert and their origins based on back-trajectory analysis. PM10 data and NECI Storm Event Database were used to create a list of NAM dust storm from 2009 to 2022 and a 24-hour HYSPLIT back-trajectory was used to identify the source region and direction of dust storms. The NARR reanalysis was used to create 500 hPa charts of selected back-trajectory events to highlight the synoptic conditions present during those events. These events were broken down into four quarters with the first quarter having the highest PM10 concentrations, to the fourth quarter having the lowest PM10 concentrations. This study shows the directional movement trends based on concentration levels of a given dust storm event. This study has been published, titled as "Trajectory Analysis of Central Sonoran Desert Dust Storms" in the *Journal of Arid Environments* in December 2023 doi:10.1016/j.jaridenv.2023.105077. The co-authors on this paper are Randall S. Cerveny and Robert C. Balling Jr.

1.3.3 Case Study 3

Chapter 4 contains my study on the third subordinate research question focusing on NAM convective dust storms that form in the central Sonoran Desert and the topographic elements that control their movement through the Gila River Valley. This paper uses three different case studies using some of the highest concentration levels of PM10. To analyze dust shielding and dust funneling caused by the local topography, the local isolated mountain complexes are identified and discussed. Including the narrow passes between the mountains like the Telegraph Pass in the middle of the South Mountain Complex and the Picacho Peak Pass. A version of this paper, titled as "Topographic Dust Shielding and Funneling: North American Monsoon Case Studies for the Sonoran Desert, Central Arizona, USA" has been submitted to the *Journal of Arid Environments*. The co-authors on this paper are Robert C. Balling, Jr. and Randall S. Cerveny

1.3.4 Central findings

Chapter 5 will address the central findings of t this dissertation. In it, I will review the research questions again subsequent questions posed in this chapter. I will then review the subsequent findings of each of the three studies. At that point I will determine if my findings adequately answer the proposed research questions. Then I will suggest possible future research based on those findings to enhance our overall understand of dust storms and their movement. Finally, I will highlight some of the useful data collected over the course of this dissertation.

CHAPTER 2

SEASONALITY IN EUROPEAN RED DUST/ “BLOOD” RAIN EVENTS

This chapter explores the seasonal distribution of 549 different recorded dust rain events across Europe. This study has a version that was published, titled as: Seasonality in European red dust/ “blood” rain events. Published in the Bulletin of the American Meteorological Society on April 1, 2012 doi: 10.1175/BAMS-D-11-00142. Co-Authors on this paper are Randall S. Cerveny and Robert C. Balling, Jr.

Abstract

Sahara-derived dust rains, termed "red rains" or more macabrely "blood rains" are rare meteorological phenomena occurring across Europe. Examples of colored rains in modern scientific literature has linked blood rains to Saharan dust transport. Many of these modern investigations, using air mass trajectories, chemical analysis, and remote sensing techniques, evaluate trajectories and chemical composition of Saharan-origin-colored rains. We briefly review synoptic conditions of three specific events using the NCEP/NCAR

Reanalysis database:

*June 22, 1988: a blood rain that occurred over northern Spain,

*March 5-10, 1991: a blood rain that occurred over Sweden, and,

*April 15-18, 2005: a blood rain that occurred over Turkey.

Then, using those as seasonal examples together with synoptic analysis using the NCEP reanalysis dataset and the HYSPLIT back trajectory model, we briefly discuss on our new chronology of over five hundred recorded colored rain events (539 events) for the European continent stretching from Spain to Russia and our analysis of blood rain

seasonality (see Figure in cover letter attachment). We have determined from our database of such events that there is a pronounced seasonality to such events.

2.1 Introduction

Sahara-derived dust rains, termed “red rains” or more macabrely “blood rains” are relatively rare meteorological phenomena associated with Saharan dust transport occurring across Europe. These red rain events have been recorded throughout European history with tales of ancient or medieval “blood rains” being described by Livy, Cicero, and Geoffrey of Monmouth among others (e.g., Cerveny, 2006). As Livy noted for 181 B.C., a shower of blood fell near the Roman Senate: “In the precinct of Vulcan and Concord there was a shower of blood... Being disturbed by these prodigies and deaths, the Fathers decreed, both that the consuls should sacrifice full-grown victims to whatever gods it seemed proper." Less drastically, modern investigations of colored rains referenced in the scientific literature, such as Coz et al. (2009) utilized back trajectories of air masses, chemical analysis, and remote sensing techniques, to

evaluate the source and chemical composition of specific Saharan-origin colored rains across Europe.

Because of the phenomenon’s relative infrequency and a prevalent case-study scientific approach to such events (e.g., Franzén et al. 1994), one aspect of red rain events that has not received significant attention is the seasonality. A couple of past studies (Dessens, 1990, Burt, 1991) created preliminary frequency analyses of colored rain events for their specific regions (France, 64 events and Great Britain, 25 events). Specifically,

Lannemezan, France demonstrated seasonality such that most frequent dust fall events occurred in the summer (Dessens, 1990). Burt (1991) found that Great Britain red rain observations increased from 1968 to 1990 which might be attributed to observational bias due to increasing awareness to the phenomenon.

2.2 Dust Rain Archive

We have assembled in a new, more comprehensive red dust rain event archive consisting of a listing of 549 colored rain cases across all of Europe, including specific month/day/year occurrence. A total of 510 of these events occurred after 1900. These colored rain cases were collected from three primary sources: (a) documented published papers; (b) images of known dust transport events using satellite data by NASA‟s Earth Observatory and other imagery; and (c) limited media accounts of such phenomena. Because we are particularly concerned with seasonality, we selected events linked to terminology such as „blood‟, „red‟, „dust‟, „mud‟, or „colored‟ rain for which existed specific dates and times of year (or, in some cases, simply the month and year of the occurrence). All data, together with the relevant references to each event, can be accessed at: http://azclimate.asu.edu/bloodrain.php.

Analysis of our spatially and temporally extensive dataset of 549 events suggests that colored rain events can occur throughout the year across Europe (Figure 2.1.) but do demonstrate seasonality. Spain tends to receive the most red dust rain events due to its close proximity to the source dust from the Sahara. The maximum occurrence of colored rain events for the Iberian Peninsula region is spring (MAM) but can occur throughout the year with winter (DJF) being the least active season for such phenomenon. However,

for most of Western Europe, red rains occur most frequently in the spring and most infrequently during the summer season.

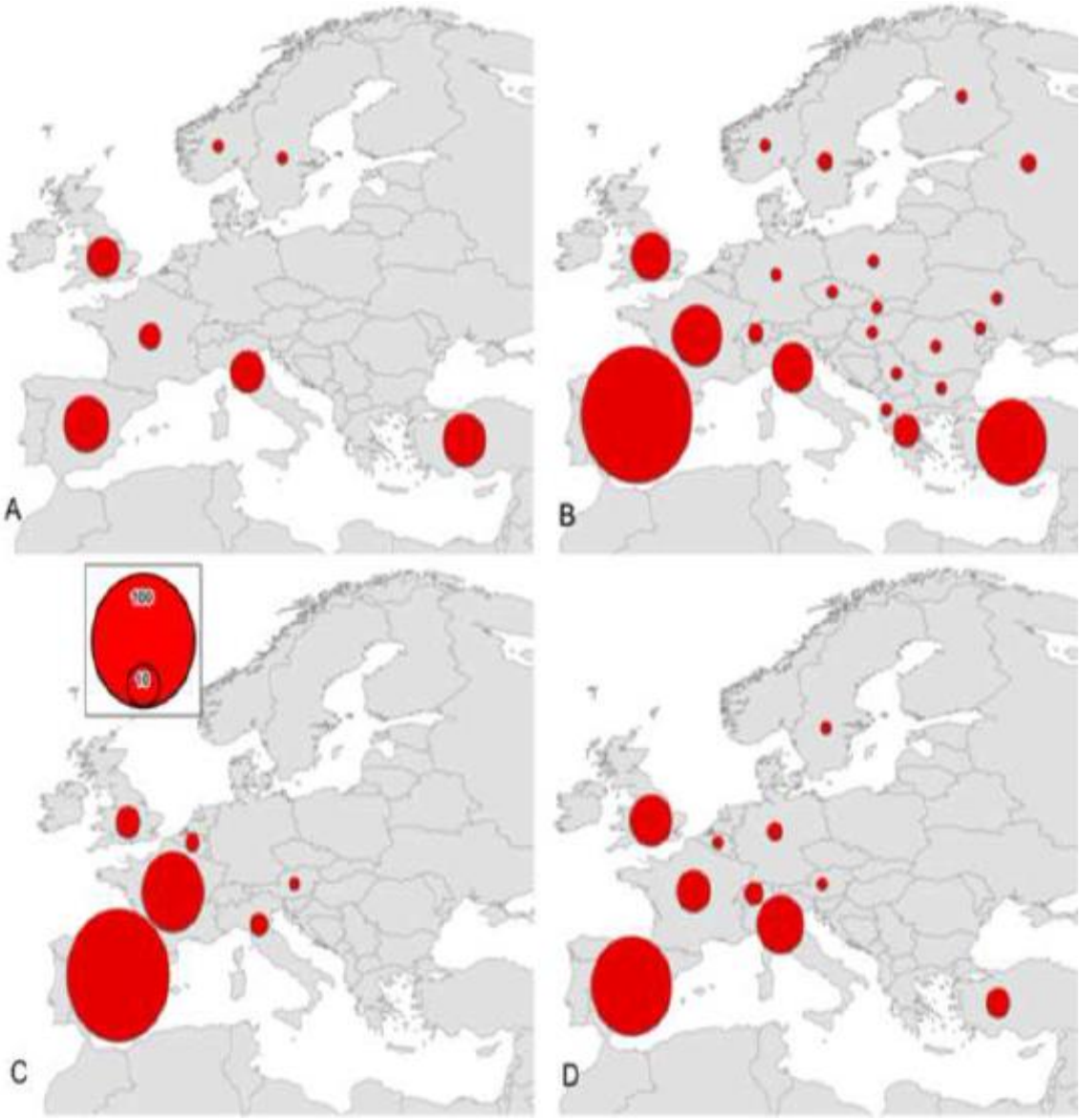

Figure 2.1. Seasonal distribution of colored rain events by country occurrence. Size of the circle over the country is proportional to the number of events recorded for that season for that country. A) Winter (DJF), B) Spring (MAM), C) Summer (JJA), D) Autumn (SON).

2.3 Case Studies

An example of the meteorological conditions for summer red rains in Western Europe (particularly Spain, France and Great Britain) can be seen (Figure 2.2.) using the NCEP/NCAR Reanalysis dataset for analysis of an event that occurred on June 22, 1988 (Kalnay et al.1996). For this June 1988 red dust rainfall, the migratory 700 hPa height field (Figure 2.2.b) over Southern Spain and Northern Morocco on the day of this event showed a low-level flow from the Atlantic that advected mid-level (700 hPa) moisture (Figure 2.2.a) into the region providing the necessary moisture for the colored rain event. The cut-off flow at the 500 hPa height (Figure 2.2.c) allowed the dust and moisture to fall over the northeastern region of Spain near Barcelona while the main downstream flow prevented it from reaching any farther into Europe. A key means of evaluating the pathway for such dust transport is through the calculation of the TOMS aerosol index (AI) (McPeters et al. 1996). The TOMS AI is a measure of how much the wavelength dependence of backscattered UV radiation from an atmosphere containing aerosols (Mie scattering, Rayleigh scattering, and absorption) differs from that of a pure molecular atmosphere (pure Rayleigh scattering) (McPeters et al. 1996). Quantitatively, the aerosol index AI is defined to be:

$$AI = 100\ log_{10}[\frac{I\frac{Meas}{360}}{I\frac{Calc}{360}}] \qquad (2.1.)$$

Where: $I\frac{Meas}{360}$ is the measured 360 nm EP-TOMS radiance, and $I\frac{Calc}{360}$ is the calculated 360 nm EP-TOMS radiance for a Rayleigh atmosphere. Under most conditions, the AI is

positive for absorbing aerosols such as Saharan dust, and negative for nonadsorbing aerosols (pure scattering).

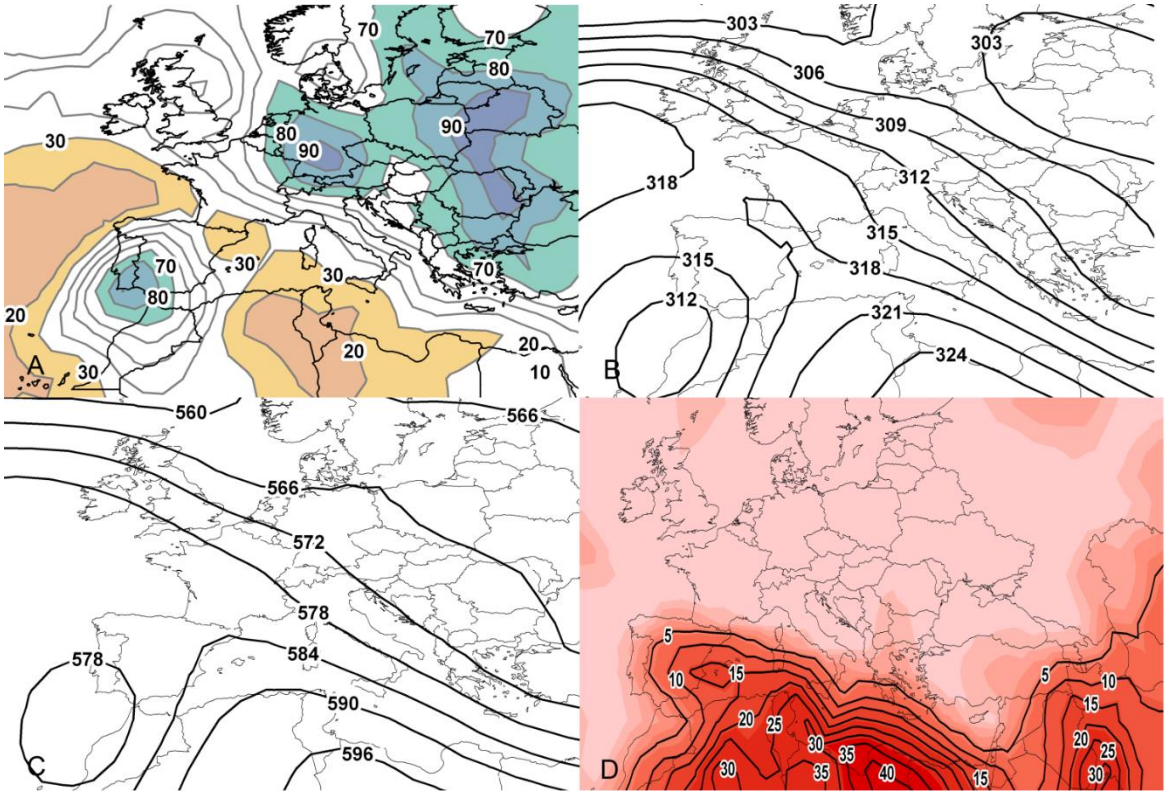

Figure 2.2. Synoptic situation associated with red precipitation event over Wesern Europe on 12 UTC June 22, 1988. (A) NCEP/NCAR Reanalysis 700 hPa relative humidity (percent); (B) NCEP/NCAR Reanalysis 700 hPa height contours (decameters); (C) NCEP/NCAR Reanalysis 500 hPa height contours (decameters); (D) TOMS Aerosol Index values (unitless).

For the June 22, 1988 event, the TOMS AI displays high aerosol concentrations extending throughout the affected region (Figure 2.2.d). Sensors collected fallen red rain samples in the northeastern region of Spain near Barcelona in a holm oak forest (Montsery). This region often receives such events and the forest itself depends on the influx of calcium supplied by these events (Avila et al. 1998). Although occurring during the summer, this pattern is actually typical for most red rain events occurring in western

Europe, particularly Spain, as noted by Avila and colleagues (Avila et al. 1997; Avila and Peñuelas 1999). Such an upper-level pattern allows for dust pick-up and transport from the Morocco/Algeria region, which is a source region for the dust (Coz et al. 2009).

To demonstrate the specific path of that transport, we employed the HYSPLIT (Hybrid Single-Particle Lagrangian Integrated Trajectory) model to compute back trajectories using gridded data from NCEP/NCAR Reanalysis dataset (Draxler 1999). This Lagrangian model uses dispersion for a specified particle or puff so that it can be viewed as a simple trajectory requiring only a three-dimensional velocity field (Draxler and Hess1997 and 1998). This allows the source regions for each of our colored rain events to be identified, and to provide the most likely track that the particulates traveled to reach their final destination. To run the analyses, we used the HYSPLIT system via READY (Real-time Environmental Applications and Display sYstem), which is a web-based system linked to a world network of data run through the Air Resources Laboratory at NOAA (Draxler and Rolph 2011; Rolph 2011). Figure 3.3.a displays the results of the June 22, 1988 Spanish blood rain back trajectory analysis. This analysis reveals that the parcel's vertical assent is one of the most significant aspects of the dust transport. For all three cases, the terminal 3500m level represents the parcel's location within the precipitating cloud layer at the specific event location. Backtracking from that terminal height, each trajectory shows that these parcels not only originated over the identified source region, but also developed very close to the surface. In this Spanish rain event, as well as the Swedish example discussed below, the initial heights in Africa were below

500m. This strongly reemphasizes that substantive surface dust can be uplifted and advected into Europe to be deposited as colored rain.

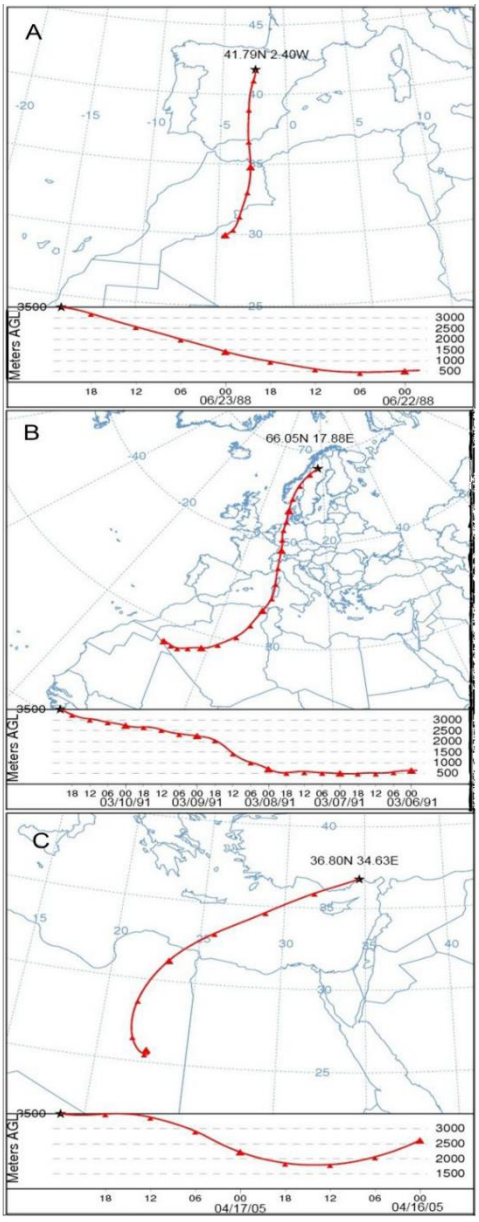

Figure 2.3. NOAA HYPSLIT back trajectory model results for three “blood rain” events. (A) Montseny, Spain (June 23, 1988), 48-hour duration simulation, starting height: 3500 m AGL, (B) Arjeplog, Sweden (March 10, 1991), 120 hours duration simulation, starting height: 3500 m AGL, (C) Mersin, Turkey (April 18, 2005), 48 hours duration simulation, starting height: 3500 m AGL.

In contrast to the rather consistent seasonal distribution of red rain events in the Iberian Peninsula region, Central Europe tends towards a bimodal seasonal distribution with the majority of its events occurring in spring and autumn. For example, the NCEP/NCAR Reanalysis 700 hPa circulation associated with the red snow event over Sweden on March 10, 1991 indicates event began with a trough at the 700 hPa height centered west of France (Figure 2.4.b). Mid-level (700 hPa) moisture can also be seen moving around the trough from the Adriatic Sea (Figure 2.4.a). This low-level moisture mixed with the aerosols resulting in red and yellow colored snowfall. At 500 hPa, a large cutoff low was positioned over the Atlantic Ocean west of France (Figure 2.4.c). Because of the magnitude and positioning of the upper-level trough, dust was advected from the central Sahara to Sweden, as evidenced by the high values of the TOMS Aerosol Index extending from the Mediterranean across central Europe (Figure 2.4.d). The yellow snow fell in northern Sweden in the city of Arjeplog and in Finland, which was confirmed by several collection samples set up throughout the Alps (Franzén et al. 1994). This type of dust storm event allows dust entrainment from the Morocco/ Algeria region as identified by Coz and colleagues and by Franzén and colleagues (Coz et al. 2009; Franzén et al. 1994) and the HYSPLIT back trajectory simulation (Figure 2.3.b). This event demonstrated a southerly flow thereby allowing the dust to be carried through central Europe into Northern Scandinavia and deposited as a yellow snow.

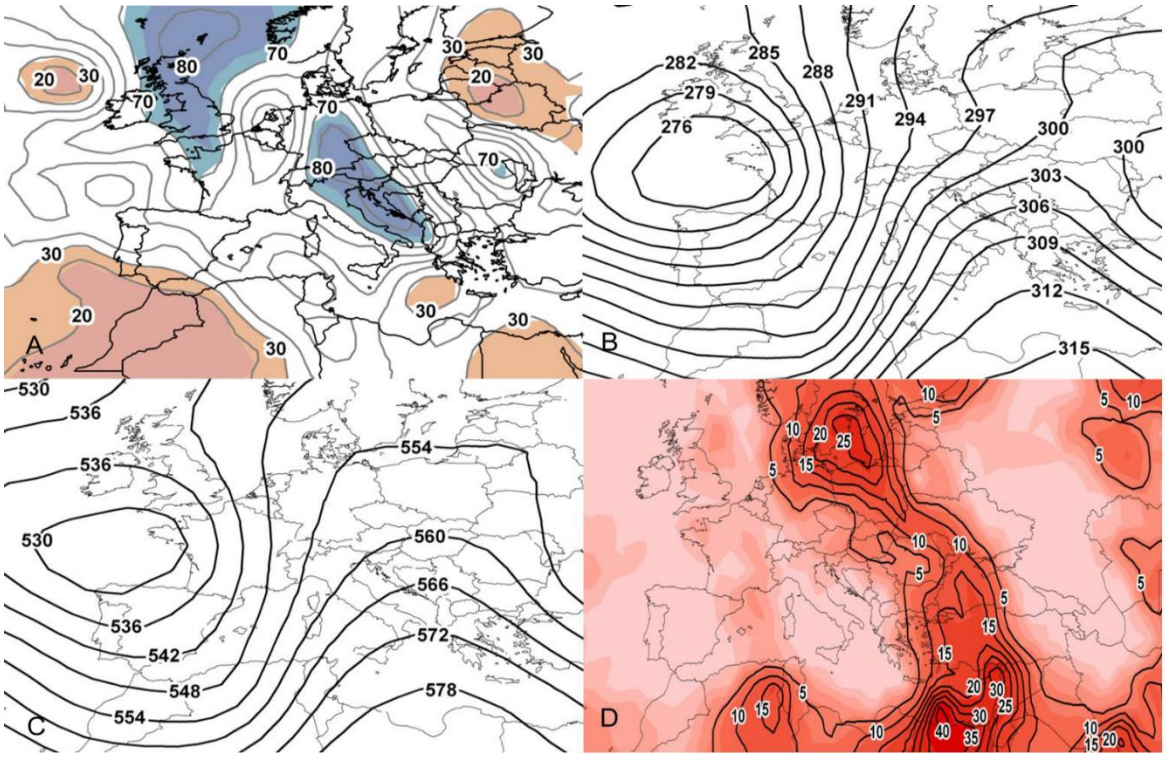

Figure 2.4. Synoptic situation associated with red precipitation event over Sweden on 12 UTC March 10, 1991. (A) NCEP/NCAR Reanalysis 700 hPa relative humidity (percent); (B) NCEP/NCAR Reanalysis 700 hPa height contours (decameters); (C) NCEP/NCAR Reanalysis 500 hPa height contours (decameters); (D) TOMS Aerosol Index values (unitless).

Seasonally, Eastern Europe, particularly Turkey, Greece, and Russia, experience the majority of its colored events in spring. For example, the NCEP/NCAR Reanalysis 500 hPa circulation associated with the red rain event across Turkey on April 18, 2005 shows that the day of the red rain event a 500 hPa cutoff low established over northern Italy (Figure 2.5.c). Additionally, the cutoff low was also evident at low level 700 hPa over northern Italy advecting both moisture from the Mediterranean and dust entrainment from the Algeria/Libya region, which is a source region identified by Coz et al. (2009) and confirmed by the HYSPLIT back trajectory simulation (Figure 2.3.c). By the day of the event, the TOMS AI indicates high concentrations of particulates over Turkey (Figure

2.5.d). The red rain that fell in the city of Mersin was identified by several samples collected from sensors around that city which sits on the edge of the Mediterranean Sea (Özsoy and Örnektekin 2009).

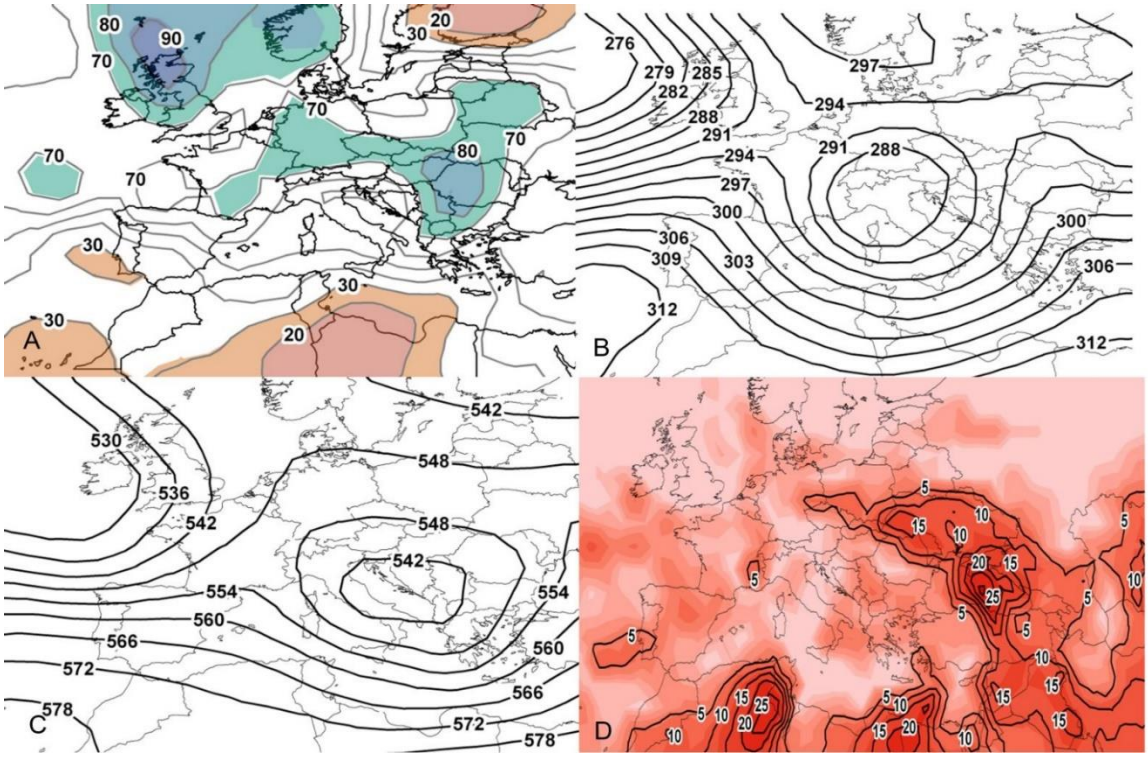

Figure 2.5. Synoptic situation associated with red precipitation event over Eastern Europe on 12 UTC April 18, 2005. (A) NCEP/NCAR Reanalysis 700 hPa relative humidity (percent); (B) NCEP/NCAR Reanalysis 700 hPa height contours (decameters); (C) NCEP/NCAR Reanalysis 500 hPa height contours (decameters); (D) TOMS Aerosol Index values (unitless).

2.4 Discussion and Conclusions

Consequently, the climatological synoptic conditions responsible for the geographic variability in the seasonality of European red rain events is seen to be linked to the interaction between migratory Rossby waves (often in the form of stagnant or quasi-stationary cutoff lows that persist long enough to force particulates northward across the

Mediterranean or western Atlantic) combined with aerosol uplift from three distinct North African source regions. While attributes of any individual event might be created due to sudden synoptic shifts in storm track and intensity of the overlying storm system, our analyses of the past century's red rain events suggest a climatic consistency to the seasonality and synoptic conditions of these phenomena.

Although these events have not created injury or marked property damage, climatological tabulation of such events may provide a new gauge of climate change because of their past relative rarity. If, as new events are noted and analyzed, changes are in the seasonality, magnitude, or overall frequency are discovered, such changed may provide valuable information on shifts in circulation and dust mobility, at least over the Eastern Hemisphere. Consequently, we stress that this is a first attempt to establish a continental-scale database for red rain events and that citations for additional events are welcomed. The data, together with the relevant references to each event, can be accessed at: http://azclimate.asu.edu/bloodrain.php. Because of the rarity and visually unconventional (or, to some, frightening) appearance, the colored rain phenomenon across Europe is likely to continue to be the source of interesting scholarly work as well as of marked interest by the general public.

Acknowledgments.
We thank the many scientists involved in red rain case studies for their data and, in particular, Dr. Turkan Özsoy of Mersin University, Turkey for colored rain data for Turkey. We greatly appreciate a reviewer's suggestion to conduct the HYSPLIT back trajectory simulations as well as additional suggestions by the editor.

CHAPTER 3

TRAJECTORY ANALYSIS OF CENTRAL SONORAN DESERT DUST STORMS

This chapter examines the summertime convective dust storms that form in the central Sonoran Desert and their origins based on back-trajectory analysis. A version of this study has been published, titled as "Trajectory Analysis of Central Sonoran Desert Dust Storms". Published in the Journal of Arid Environments in December 2023 doi:10.1016/j.jaridenv.2023.105077. Co-Authors on this paper are Randall S. Cerveny and Robert C. Balling Jr. The data sources and software used in this analysis can be found in Appendix A.

Abstract

Dust storms are a major cause of central Sonoran Desert weather fatalities. Through back-trajectory analysis of North American Monsoon dust storms in central Sonoran Desert of the United States. The focus of this study is specific to central Arizona (USA) from 2009 to 2022 using the HYSPLIT model. Our findings have shown that dust storms tend to originate from south with ninety percent of the central Arizona events developing from southerly or near-southerly regions. The dust storms displaying the highest concentrations of particulates show a preference to originate from the southwest. This coincides with the development of a 500hPa ridge to the east of the study area. The highest concentration storms' back-trajectories display the lowest heights above the ground. Given their southwestern origin, these storms travel upslope along the seasonally dry river beds of the Gila River and its tributaries. Weaker dust storms originate over a wider area with a shift to a southerly direction. Such origination indicates that weaker

dust storms are traveling downslope through the many smaller washes and channels of the dry Santa Cruz River. As dust concentrations drop, storm direction drifts east and dust height is suspended higher. This paper highlights the spatial variations in central Arizona dust storms, showing the likeliest paths of the strongest events and assists in identifying aeolian dust origins.

Significance Statement

The purpose of this study is to identify source regions of dust storms impacting the central Sonoran Desert located in the Arizona region of the Southwestern United States. Using a back-trajectory model, we find that most large dust storms impacting central Arizona have a southwestern origin, having traveled upslope along the normally-dry Gila River and its tributaries.

3.1 Introduction

Dust storms are major features of central Sonoran Desert, especially during the North American Monsoon (NAM) in which large haboobs can be generated. These dust storms produce a variety of challenges to Arizona (USA). Dust storms are the third largest cause of weather fatalities in the state, behind extreme heat/cold and flash flooding (Mohebbi et al. 2019). They produce episodes of near-zero visibility leading to auto accidents (Mohebbi et al., 2019, Tong et al. 2023). For example, highway corridors around Maricopa County (such as Interstate 10) in central Arizona have been the focus of many studies and dust detection and visibility projects and campaigns (Mohebbi et al., 2019; Reid et al., 2015). Additionally, in some places, a significant proportion of the dust

comes from croplands; simulations of dust storms have shown cropland erosion was responsible for over 50 percent of the PM10 values over Phoenix (Joshi 2021). The loss of soil can lower nutrients and cause economic hardships for farmers.

Tong et al. (2023) indicated that traditional reporting of dust storm fatalities across the United States is severely undercounted, and merging Storm Event data with Fatality Analysis Reporting System (FARS) data show 232 deaths from 2007- 2017. There are also increases in regional infection due to Valley fever being prominent in the soil throughout (Tong et al. 2017). As was the case with the other dust sources, increased morbidity rates and hospitalization due to cardiovascular and respiratory issues increase during dust events (Achakulwisut et al. 2018).

In this paper we have combined information from the NOAA Storm Event Database with EPA PM10 hourly reported data to build a catalog of dust storm events from 2009-2022. Those storms have been used to create back-trajectories of events based on concentration levels to establish a hierarchical Quarter system to determine from where directions the most intense dust storm originate. Identifying these paths will aid first-responses and forecasters in handling the impacts of these dust storms in central Arizona.

3.2 Research Area and Past Research

Our study area is confined to Maricopa and Pinal counties in south-central Arizona (Figure 1). Most dust storm events terminate within this region due to the surrounding mountain ranges preventing long range transport. However, some long-range transport onto the Colorado Plateau is possible from areas all around southern Arizona and Mexico

(Reynolds et al. 2001, Reynolds et al. 2006). This means that generally, dust storm events are produced within the Sonoran Desert. The Sonoran Desert is the second largest desert in North America and reaches from northcentral Mexico around the Gulf of California into southern Arizona and southwestern California (Figure 3.1.).

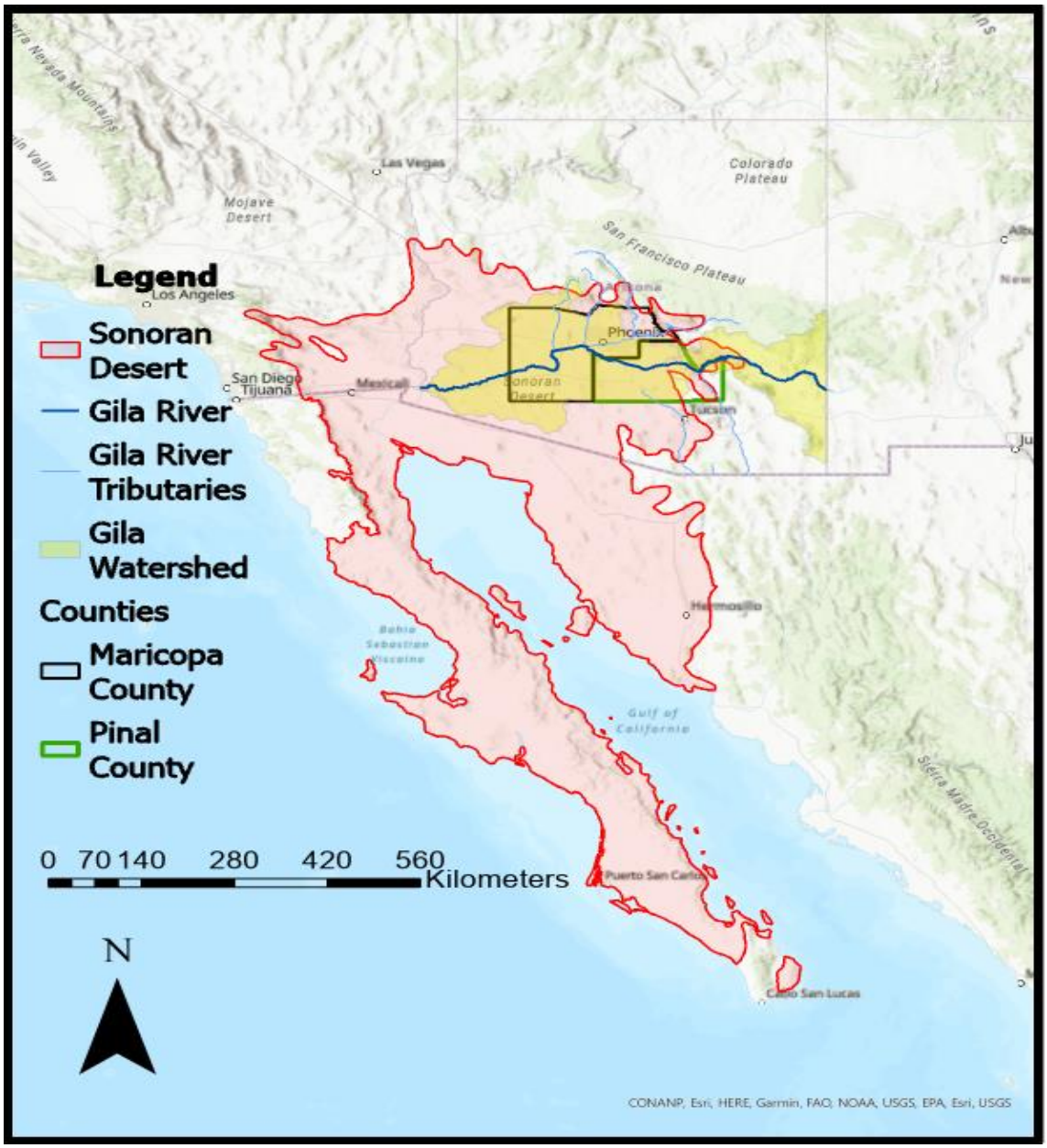

Figure 3.1. Sonoran Desert Region (highlighted in red) of Southern Arizona and Northwestern Mexico with the study areas of Maricopa and Pinal Counties (highlighted in black and green). Gila River and Tributaries and the established watershed also shown (Dark blue for Gila River, light blue for tributaries, yellow for watershed.

Drought is a major cause for increased dust production in arid and semi-arid regions such as the Sonoran Desert (Gillette and Hanson 1989, Moulin and Chiapello 2004). There are two types of airborne dust events (NWS, 2009). The first type involves blowing dust,

which is a concentration of atmospheric sand or dust that reduces visibility by 0.4 kilometers (0.25 miles) or less. The second type of event is a dust storm (or haboob) which is a concentration of atmospheric sand or dust that reduces visibility by half a mile or less and with wind speeds of 30 mph (13.4 ms-2) or more. This research focuses on the second type of dust event, i.e., dust storms.

Convective dust storms are the largest contributor to the aeolian dust output in the central Arizona portion of the Sonoran Desert (Brazel and Nickling 1986). During the summer months, and specifically during the North American Monsoon (NAM), it is common for severe thunderstorms to develop over the Central Arizona Sonoran Desert (Maddox, et al. 1995, Wallace et al. 1999). Topography of this part of the Sonoran Desert leads to thunderstorm development along the surrounding mountain ranges due to the atmospheric lifting along those ranges and the advection of moisture from the south, which is typical of NAM (Maddox et al. 1995).

The Phoenix metropolitan area in Maricopa County Arizona lies in a confluence region of several major riverbeds (although the streams are seasonally intermittent) where the gravity outflows of thunderstorms can collide and merge. Such gravity outflow can pass, for example, over a large playa or uncultivated farmland. Superimposed upon the regular NAM weather patterns that influence dust storm events in the Sonoran Desert, there is also a dust storm signal relating to the El Niño Southern Oscillation teleconnection or ENSO (Okin and Reheis 2002, Cook et al. 2007). Specifically, research indicates that there is a link to dust storms through the La Niña portion of the cycle involving the cooling of equatorial waters of the Pacific Ocean (Cook et al. 2007). The La Niña aspect

of the ENSO cycle leads to drought conditions throughout the southwestern United States (Okin and Reheis 2002, Reheis 2006). These elements combine to create a dynamic and seasonally varied monsoonal dust storm season.

3.3. Data

Our focus is on two Arizona counties in the north central region of the Sonoran Desert, specifically Maricopa and Pinal Counties (Figure 1). The data for this analysis are collected from two major sources, the Storm Event Database provided by the National Oceanic and Atmospheric Administration (NOAA) and the Hourly Particulate Matter 10 micrometers (PM10) data from the Environmental Protection Agency (EPA). These sources provide day, time, location, and concentration data for dust storm events within the period of 15 June – 30 September from 2009 to 2022. This follows current NWS guidelines that give specific start/end dates to the National Oceanic and Atmospheric Administration.

The Storm Event Database provides a basic classification for a dust storm event by county with detailed spotter accounts of these event (Murphy 2021). Any day flagged as a dust storm event in Maricopa or Pinal Counties was added to the list of events. As an example, data from Arizona for the 5 July 2011 Dust storm event, one of the largest to hit the region in modern records is shown in Table 3.1.

Location	County	St.	Date	Time	T.Z.	Type	Mag	Dth	PrD	CrD
Totals:							n/a	0	720.00 K	0.00 K
CENTRAL DESERTS (ZONE)	CENTRAL DESERTS	AZ	7/5/2011	18:30	MST-7	DS	no data	0	0.00 K	0.00 K
GREATER PHOENIX AREA (ZONE)	MARICOPA CO.	AZ	7/5/2011	19:20	MST-7	DS	no data	0	30.00 K	0.00 K
GILA BEND	MARICOPA CO.	AZ	7/5/2011	19:30	MST-7	TSTM	57 kts.	0	0.00 K	0.00 K
OCOTILLO	MARICOPA CO.	AZ	7/5/2011	19:32	MST-7	TSTM	60 kts.	0	80.00 K	0.00 K
HIGHTOWN	MARICOPA CO.	AZ	7/5/2011	19:45	MST-7	TSTM	51 kts.	0	0.00 K	0.00 K
FALFA	MARICOPA CO.	AZ	7/5/2011	20:30	MST-7	TSTM	50 kts.	0	10.00 K	0.00 K
VALENCIA	MARICOPA CO.	AZ	7/5/2011	20:30	MST-7	TSTM	70 kts.	0	600.00 K	0.00 K
Totals:							n/a	0	720.00 K	0.00 K

Table 3.1. Sample of the Storm Event Database from 5 July 2011. Table from left to right: Location, County/ Zone of event, State (AZ), Date of the event (5/7/2011), the time for each observation, Time Zone (Mountain Standard Time), Type of Storm, recorded wind speed Magnitude (knots), Death Count for event, Injuries for event, Estimated Property Damage, and Estimated Crop Damage.

The EPA's hourly particulate matter at or less than ten microns in diameter (PM10) data are the second main dataset used in this study. Through the Clean Air Act, the EPA has set specific criteria and standards for dust monitoring (EPA, 2007). This is accomplished through state agencies in a hierarchical format. For Arizona, the Arizona Department of Environmental Quality (ADEQ), and at the county level the Maricopa County Air Quality Department (MCAQD) and the Pinal County Air Quality Department (PCAQD) handle particulate measurements.

Each data source is subject to caveats to their use. For example, the storm event database has some reliability issues due to human error in data collection, leading to an incompleteness and inconsistency of the data (Santos 2016). Similarly, the hourly PM10 network is spaced inconsistently and individual counties do set different data collection thresholds depending on the type of monitor used, which Maricopa and Pinal counties do. According to the Arizona Department of Environmental Quality, they use a Beta attenuation monitoring (BAM) set at 5000 μgm-3 for accuracy. However, the present head Pinal County Air Quality department and from the past head of Maricopa County Air Quality state that their counties use Tapered Element Oscillating Microbalance (TEOM) with no upper threshold set.

Consequently, sensors in one location may not be compatible with sensors in another location. In Arizona, Pinal County air quality sensors have a greater range in PM10 monitoring than do their Maricopa County counterparts. For example, hourly air quality values in Pinal County have been recorded as high as 35,000 μgm-3. However, hourly air

quality concentrations in Maricopa County typically do not reach above 5000 μgm-3. Therefore, the two counties' dust storms are treated separately.

3.4. Methods

The Storm Event Database and the hourly PM10 data are combined by county, time of event, and concentration levels to create two separate datasets of dust storm occurrence. We will classify the dust storm events for the two counties into four categories by concentration level. From 2009 to 2022, Maricopa County recorded 71 different dust storm events while Pinal County recorded 83 events. These events were classified by concentrations such that the 'Quarter One' events comprise the top quarter of dust storms by concentration, 'Quarter Two' events comprise the 50-75 percent of dust storms by concentration and soon. Quarter One events, the top 18 based on concentration, are shown in Table 3.2. These data are used to create a back-trajectory analysis based on concentration levels.

Date Local	Time Local	Date GMT	Time GMT	Samp., Measurement
7/5/2011	20:00	7/6/2011	3:00	6348
6/30/2013	23:00	7/1/2013	6:00	5251
6/27/2012	20:00	6/28/2012	3:00	4985
8/2/2018	19:00	8/3/2018	2:00	4663.5
8/18/2011	18:00	8/19/2011	1:00	4373
9/7/2017	19:00	9/8/2017	2:00	4293
8/7/2018	22:00	8/8/2018	5:00	4007
7/22/2019	22:00	7/23/2019	5:00	3964
7/9/2021	23:00	7/10/2021	6:00	3957.5
7/9/2018	0:00	7/9/2018	7:00	3649
8/11/2012	17:00	8/12/2012	0:00	3351
8/8/2018	20:00	8/9/2018	3:00	3320
8/26/2013	19:00	8/27/2013	2:00	3242

8/16/2020	18:00	8/17/2020	1:00	3216
9/6/2012	17:00	9/7/2012	0:00	3056
7/3/2014	21:00	7/4/2014	4:00	2872
7/29/2016	19:00	7/30/2016	2:00	2864
7/18/2011	18:00	7/19/2011	1:00	2861

Table 3.2. Quarter 1 (Top quarter of all events, 18 dust storms) events by dust concentration (μgm-3).

3.4.1 HYSPLIT Model

To demonstrate the specific path of transport for each of our events we employ a Hybrid Single-Particle Lagrangian Integrated Trajectory (HYSPLIT) model to compute back-trajectories using gridded data from the Global Data Assimilation System (GDAS) dataset (Stein et al. 2015). This Lagrangian model uses dispersion for a specified particle or puff so that it can be viewed as a simple trajectory requiring only a three-dimensional velocity field. This method allows the source regions for each of our dust storm events to be identified, and to provide the most likely track that the particulates have traveled to reach their destination (e.g., White et al. 2012). To run the analyses, we used the HYSPLIT system via the Real-Time Environmental Applications and Display System (READY), which is a web-based system linked to a world network of data run through the Air Resources Laboratory at NOAA (Rolph et al. 2017). An example of a HYSPLIT model run for the exceptional 5 July 2011 dust storm event (NOAA, 2023a) showing the meters above ground level (AGL) height is given in Figure 3.2.A. Since data for each county were obtained from various sources around their respective counties a centralized point (Maricopa County: Sky Harbor Airport; Pinal County: Casa Grande Regional Airport) was chosen to represent each county to normalize the results.

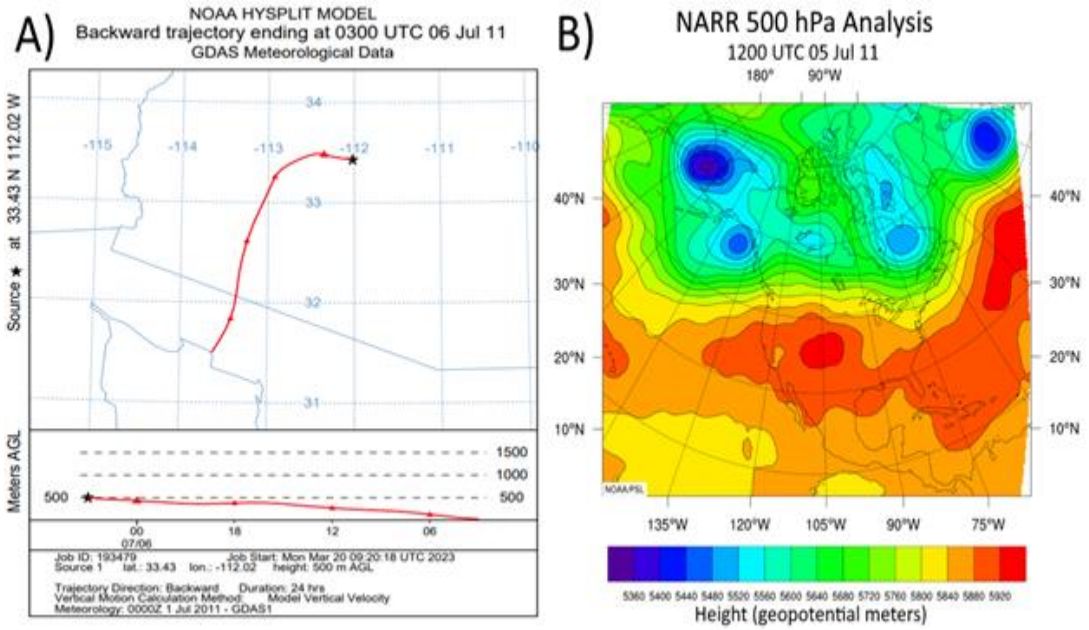

Figure 3.2. A) Back-trajectory plot for the 5 July 2011 dust storm with ending point at Barry Goldwater Sky Harbor Airport (PHX) with a 24-Hour duration. Meters AGL not reaching above 500m. B) NARR 3-Hour 500 hPa Geopotential height in meters for 12 UTC, 5 July 2011, approximately two hours before the dust storm event

3.4.2 North American Regional Reanalysis (NARR)

In conjunction with the HYSPLIT data, we also compared the overall synoptic atmospheric conditions for these dust storm events. We selected the North American Regional Reanalysis (NARR) reanalysis model as being most applicable for our region (Mesinger et al. 2006). It is a reanalysis model that can identify low level moisture and air flow (700 hPa level) and upper air movement (500 hPa level) associated with the synoptic conditions of dust storm events. Below is an example of the 500 hPa (500 mb) Geopotential height map for the exceptional 5 July 2011 dust storm event (NOAA, 2023b) (Figure 3.2.B). This demonstrates for that extraordinary dust storm, the presence

of a large subtropical ridge located in the central Rocky Mountains which provided upper-level support for southwesterly flow over central Arizona.

3.4.3 Geographic Categorization

To better identify source regions and likely paths for dust storm events, we have segregated each county in relation to a focal point associated with its centrally located airport and major weather station (Maricopa Sky Harbor Airport, Pinal Casa Grande Regional Airport respectively). We divided the area into eight distinct regions based on cardinal directions (e.g., West, North-West, North, North-East, East, South-East, South and South-West). Each circle has a radius of approximately ~644 km, and each region has an area of approximately ~96270 km2 (Figures 3.3. and 3.4.). Each event is plotted by the hour to identify hourly contact within each region and to discern patterns based on latitude, longitude, and height. The subsequent analysis will be based on these methods.

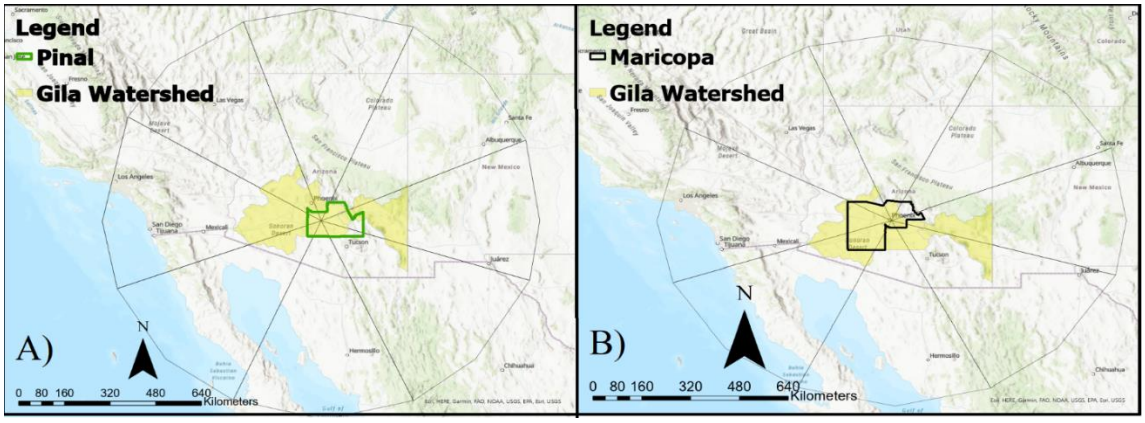

Figure 3.3. (A) Pinal County directional identifier for Dust Storm Initiation (West, North-West, North, North-East, East, South-East, South and South-West) from central focal point, Case Grande Regional Airport. Circle radius 400 mi., (643.7 km), average regional area 59,820 mi2, (96271 km2) (B) Maricopa County directional identifier for Dust Storm Initiation (West, North-West, North, North-East, East, South-East, South and South-West) from central focal point, Sky Harbor Airport.

3.5. Results

The dust storm analyses have been broken down by county and separated into four Quarters based on quarterly distribution of concentration levels (e.g., ‘Quarter 1’ is the top quarter of dust storm events by concentration, Table 3.2.). Each Quarter shows specific directional patterns, which are similar for both counties. We discuss the synoptic patterns that present for the assigned cardinal regions by concentration quarter, and then discuss the back-trajectories of specific storms.

3.5.1 Synoptics

NAM dust storm events are often generated by the outflow of convective thunderstorms. Convective dust storms are the largest contributor to the aeolian dust output in the central Arizona portion of the Sonoran Desert (Brazel and Nickling 1986). These conditions are created by the summertime subtropical high pressure that generally sets up over the central parts of the country and drives anticyclonic motion from the Gulf of California towards the Central Sonoran Desert (Maddox et al. 1995, Wallace et al. 1999). The exact position and intensity of the subtropical high affects the movement of dust storm events. To highlight that influence, the synoptics of sample dust storms displaying the highest PM10 concentrations are shown below (Figure 3.4.). Approximately 90 percent of all dust storms examined come in from these four regions (W, SW, S, SE)

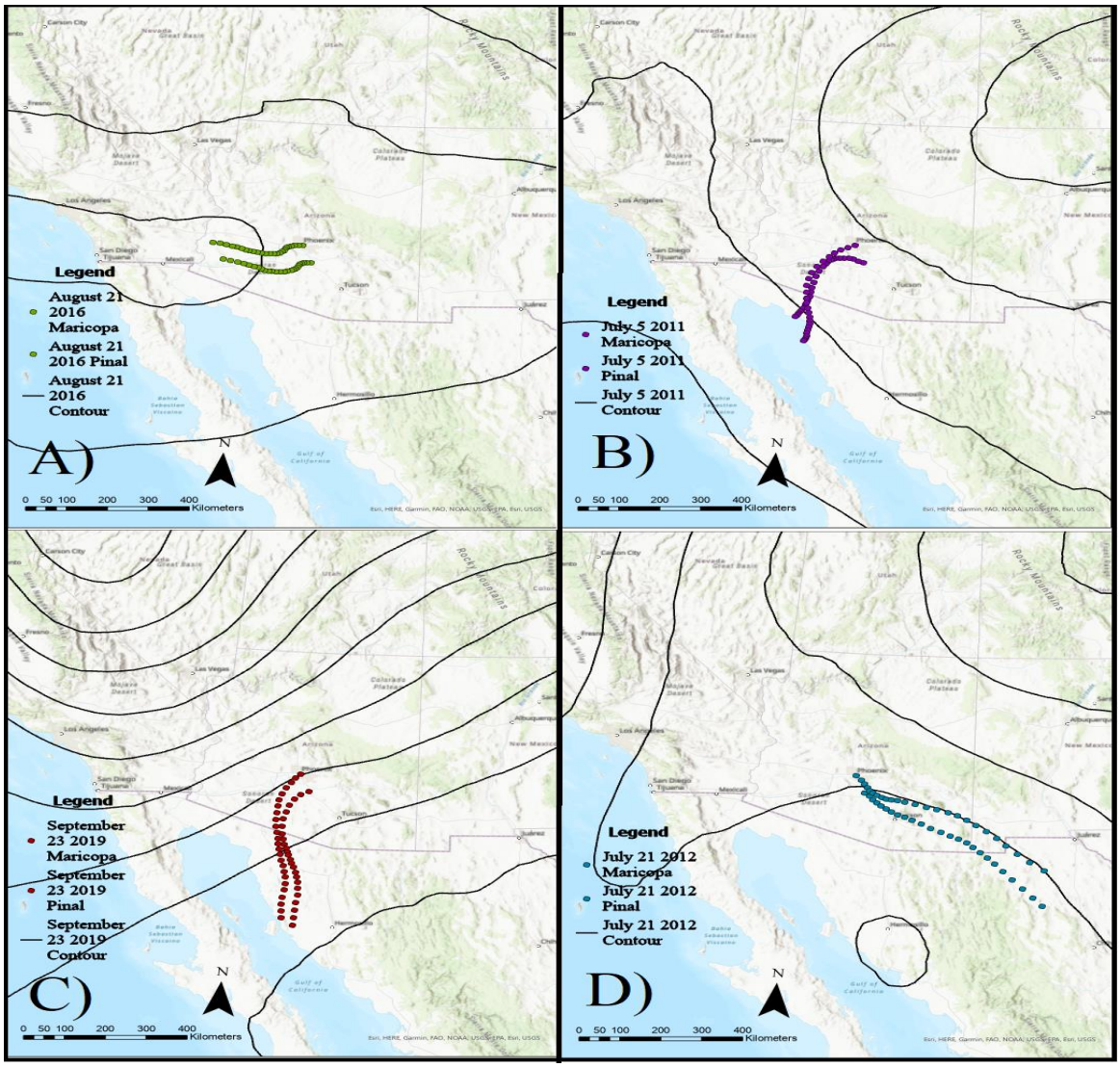

Figure 3.4. A) The trajectory and 500 hPa height field associated with the 21 August 2016 dust storm from Phoenix Sky Harbor and Casa Grande Regional Airports with geopotential height at 500hpa B) The trajectory and 500 hPa height field associated with the 5 July 2011 dust storm at Phoenix Sky Harbor and Casa Grande Regional Airports C) The trajectory and 500 hPa height field associated with the 23 September 2019 dust storm at Phoenix Sky Harbor and Casa Grande Regional Airports D) The trajectory and 500 hPa height field associated with the 21 July 2012 dust storm at Phoenix Sky Harbor and Casa Grande Regional Airports.

3.5.1.1 West

Figure 3.4.A displays an event that arrived into central Arizona from the West and the Southwest. The event occurred on 21 August 2016. In this mature NAM season example, the subtropical high expanded and shifted north which fits the typical synoptic pattern for NAM (Carlaw et al. 2017). This shift allowed the individual storms to flow from multiple areas and flow upslope towards the central Arizona desert.

3.5.1.2 Southwest

The events with the highest concentration levels are associated with a strong subtropical high-pressure system situated over the southwestern US and arise out of the Southwest around the Gulf of California as shown in Figure 3.4.B (5 July 2011 event). As the subtropical high pressure begins to shift away or lessen in intensity, the dust storms begin to weaken and shift direction.

3.5.1.3 South

On 23 September 2019, a northerly moving dust storm event (Figure 3.4.C) is produced from a 500 hPa short wave trough normally associated with flash flooding events (Maddox et al. 1980). That short wave trough pushes thunderstorm activity from the south towards the central Arizona desert creating dust storm activity in both Maricopa and Pinal counties.

3.5.1.4 Southeast

The 21 July 2012 event (Figure 3.4. D) shows the subtropical high pressure centered over the upper great plains with a strong 500 hPa shortwave moving across southern Arizona. The shortwave pushes the incoming winds off to the southeast where they flow downstream along the Santa Cruz River Valley into the central deserts of Arizona.

3.5.2. Dust storm movement

Dust storm back-trajectories are plotted out by hour for a 24-hour period and overlaid onto the circular regions based on the cardinal directions. This process was employed to highlight the general direction of dust storm events as they approach each of their respective terminations (Figure 3.5.). There is considerable overlap in events for both counties but closer examination reveals some distinct differences between the counties and between the respective Quarters.

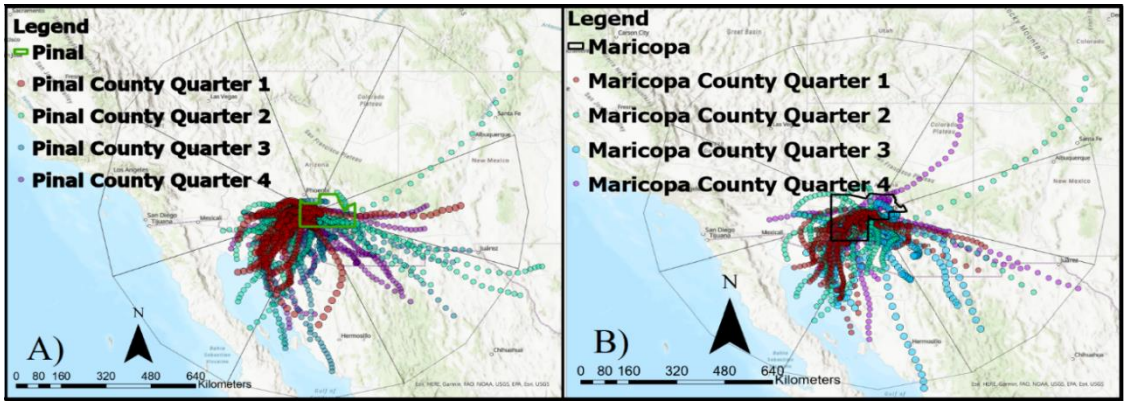

Figure 3.5. A) Pinal County hourly back-trajectories Quarters 1-4 centered on Casa Grande Regional Airport overlaid on circular regions by cardinal directions North, Northeast, East, Southeast, South, Southwest, West, Northwest. B) Maricopa County hourly back-trajectories Quarters 1-4 centered on Sky Harbor International Airport overlaid on circular regions by cardinal directions North, Northeast, East, Southeast, South, Southwest, West, Northwest.

All dust storm events were plotted for each concentration Quarter in each county for the 24-hour period leading up to the dust storm. The trajectory maps also identify the Gila River watershed and its tributaries such as the Santa Cruz River. These features highlight the connection between each of these dust storm events and the dry riverbeds and washes. Although on maps, these rivers are highlighted in blue, these channels are normally dry year-round (and particularly at the start of NAM).

3.5.2.1 Quarter 1 (maximum concentration) events

For each Quarter every hour for each event was geocoded and placed within one of the eight regions based on its cardinal position. The Quarter 1 events for Maricopa and Pinal County where then placed in a wind rose based on those cardinal directions to indicate the region that these storms arrive from. Each Quarter has its own unique profile. For both counties, Quarter 1 shows heavy concentration originating from the Southwestern region (Figure 3.6.). This is likely due to downbursts over open dry dusty river beds of the Sonoran Desert found in that region (Figure 3.7.A).

Trajectory analyses for Quarter 1 dust storms for both counties confirmed that the largest number of events coming from the Southwest region along the Gila River (Figure 3.6.A, B). Most events begin at or near the surface only rising the 500 m level by the time they reach their destinations. The only exceptions for Maricopa County (Figure 3.6.D) are the two storms that come from the Southeast with heights of 690-1031m. However, the events arriving from the Southwest are generally starting out at or near sea level by the Gulf of California. The events coming from the Southeast are moving downslope from

the higher elevated surrounding mountains. Pinal County shows a similar trend with most events beginning at or near the surface with the few exceptions coming from the Southeast and South over mountains with max heights of 575-1758m (Figure 3.6.C).

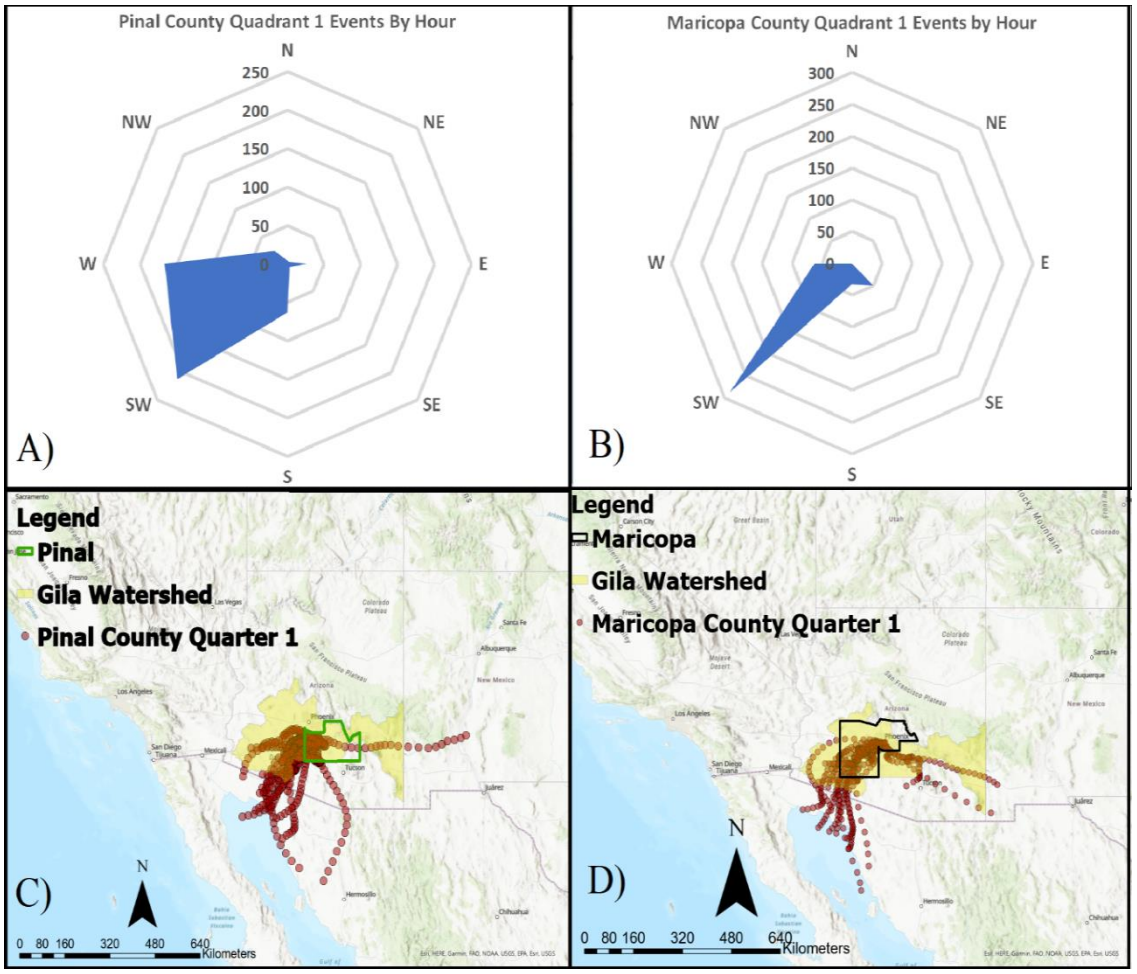

Figure 3.6. A) Pinal County Quarter 1 (top 25percent dust concentration) events wind rose plotted by hours of contact within each region B) Maricopa County Quarter 1 events wind rose plotted by hours of contact within each region C) Back-trajectory of all Quarter 1 dust storm events by latitude, longitude, and height for Pinal County over a map of Southern Arizona highlighting the Gila River watershed and its tributaries D) Back-trajectory of all Quarter 1 dust storm events by latitude, longitude, and height for Maricopa County over a map of Southern Arizona highlighting the Gila River watershed and its tributaries.

Trajectory analyses for Quarter 1 dust storms for both counties confirmed that the largest number of events coming from the Southwest region along the Gila River (Figure 3.6.A and B). Most events begin at or near the surface only rising the 500 m level by the time they reach their destinations. The only exceptions for Maricopa County (Figure 3.6.D) are the two storms that come from the Southeast with heights of 690–1031 m. However, the events arriving from the Southwest are generally starting out at or near sea level by the Gulf of California. The events coming from the Southeast are moving downslope from the higher elevated surrounding mountains. Pinal County shows a similar trend with most events beginning at or near the surface with the few exceptions coming from the Southeast and South over mountains with max heights of 575–1758 m (Figure 3.6.C).

Dust storm speed was estimated using the hourly back-trajectory locations' change in position with time for a particulate. Maricopa County storms showed a max speed range of 4.8–11.1 m s−1. Pinal County storms showed slightly slower speed max at 4.1–8.8 m s−1. Surprisingly, the events with the highest wind speeds did not produce the largest PM10 concentrations for Maricopa or Pinal Counties. This is likely the result of dust concentration linked to the path of the event rather than the wind speeds of the event. For Maricopa County the largest event was July 5, 2011 event, and the fastest wind speed was 6.2 m s−1, and Pinal County was only 3.7 m s−1 for its largest event, the dust storm of July 30, 2016.

During the summer months, and specifically during the NAM, it is common for severe thunderstorms to develop over the central Arizona Sonoran Desert (Maddox et al., 1995;

Wallace et al., 1999). Topography of this part of the Sonoran Desert leads to thunderstorm development along the surrounding mountain ranges due to the atmospheric lifting along those ranges and the advection of moisture from the south, which is typical of the NAM (Maddox et al., 1995).

Downbursts form along the mountain ridges can cause cold pool outflows which flow down mountain slopes of river basins into the valleys of the lower desert (Wallace et al., 1999). Specifically, the Gila River on the western side of Arizona is closely aligned with the strongest events in Quarter 1 (Figure 3.7. A). The Gila River and most of its tributaries are dry beds west of the Pinal mountains at the eastern edge of Pinal County. The largest dust storm events trek along the Gila River into Maricopa and Pinal Counties. This also explains why there are events in Pinal County Quarter 1 that come in from the Southwest and the West, while Maricopa County Quarter 1 has mostly Southwestern events. The Gila River itself flows from East to West, but the storms generally approach from the south. Since Pinal County is farther south than Maricopa County, the Gila River approach from a westerly direction as it gets closer to Pinal County.

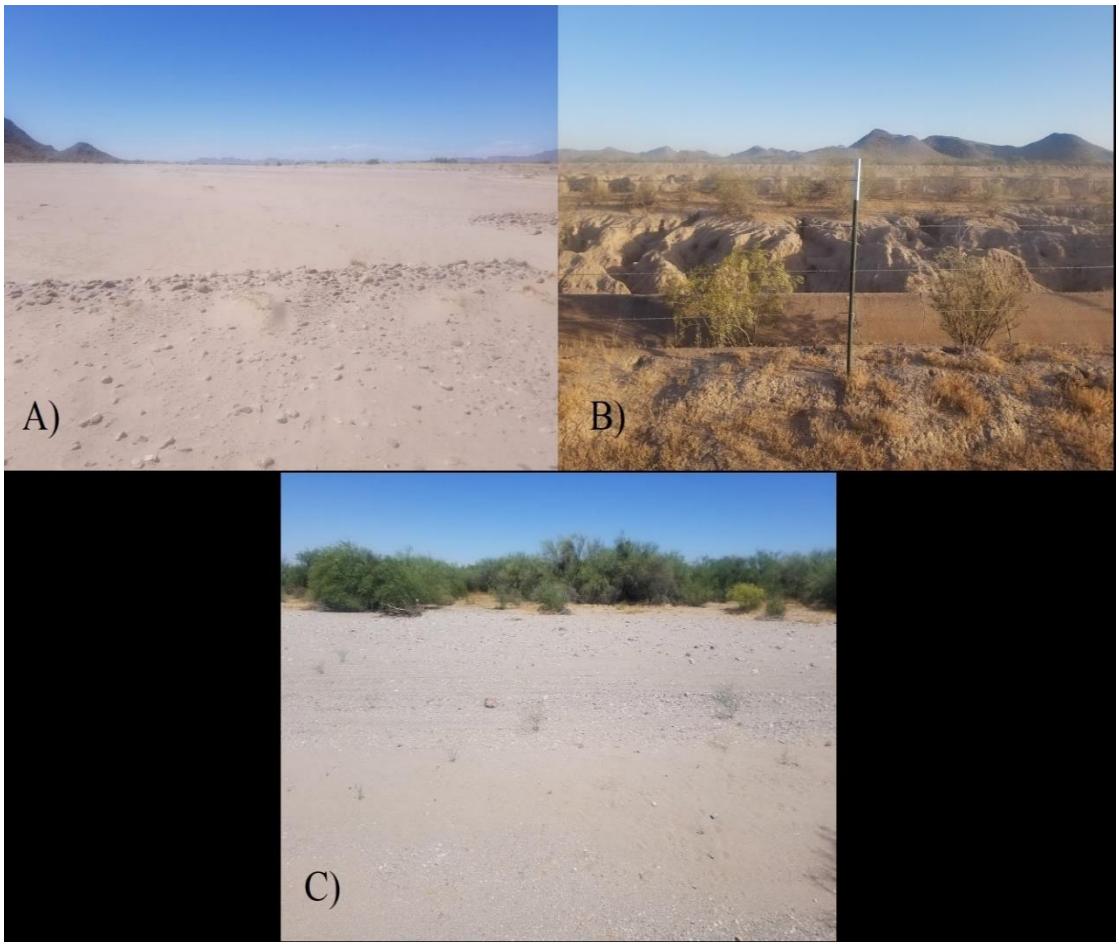

Figure 3.7. Dry Gila River bed expanse near Gila Bend, AZ. A nexus point for Southwestern dust storm events for both Maricopa and Pinal Counties. Location: 33.0538340, -112.6888150. 4 June, 2023 Taken by Lead Author.

3.5.2.2. Quarter 2 events

The group of next highest dust concentration (dust concentrations ranked 50–75 percent of all events) dust storms, Quarter 2, shows a similar large proportion of time spent over the Southwest region, and slightly less time in the West region. In contrast to Quarter 1, this group also has a few events shifting towards the Southeast (Figure 3.8.AB). The rationale for this preponderance of activity is the Southwest again is likely due to the position of the counties and the topography of the land. Most events begin at or near the

surface only rising the 500 m level by the time they reach their terminations. This Quarter contains an anomalous event for both counties in a dust storm that came down off the Colorado Plateau with a height of about 4800 m on August 17, 2020. Just as before the events arriving from the Southwest are generally starting out at or near sea level by the Gulf of California. The events coming from the Southeast are moving downslope from the higher elevated surrounding mountains.

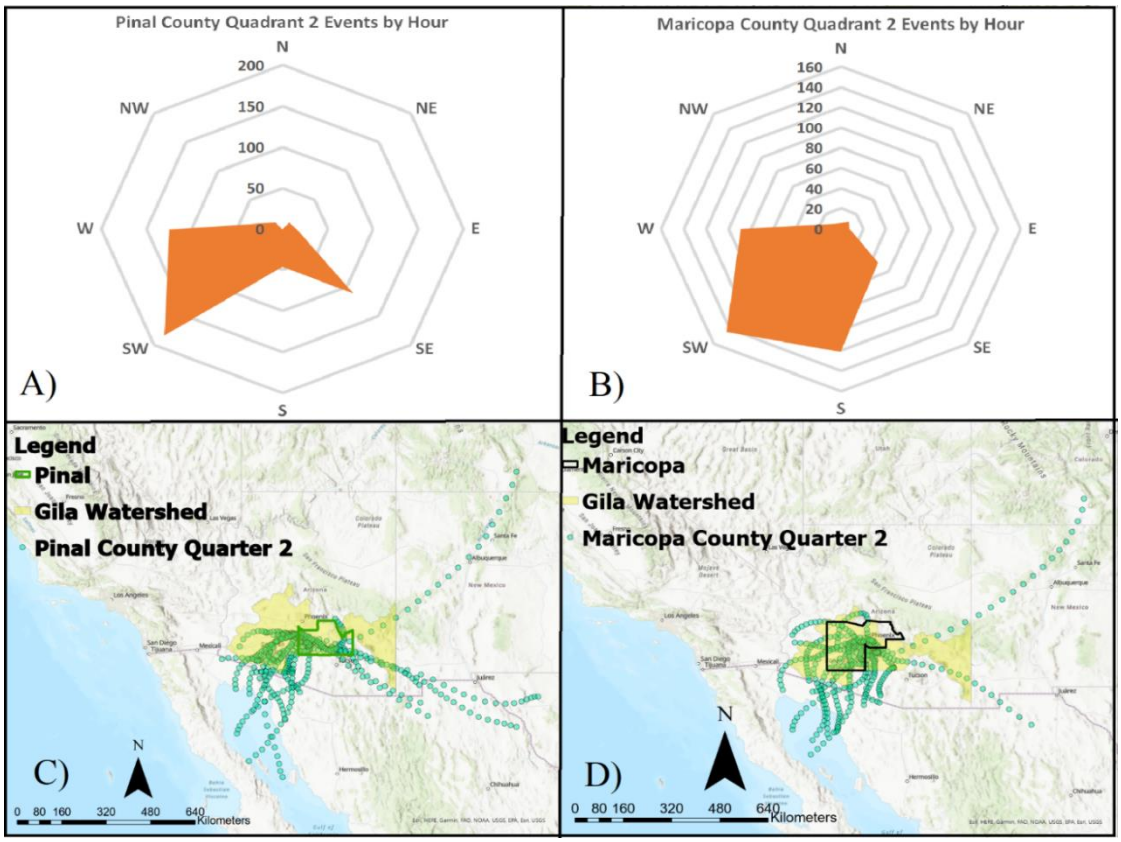

Figure 6.8. A) Pinal County Quarter 2 (50-75% of highest dust concentration events) events wind rose plotted by hours of contact within each region B) Maricopa County Quarter 2 events wind rose plotted by hours of contact within each region C) Back-trajectory of all Quarter 2 dust storm events by latitude, longitude, and height for Maricopa County over a map of Southern Arizona highlighting the Gila River watershed and its tributaries. D) Back-trajectory of all Quarter 2 dust storm events by latitude, longitude, and height for Pinal County over a map of Southern Arizona highlighting the Gila River watershed and its tributaries

Dust storm events in Maricopa County showed a maximum speed ranging from 4.7 to 12.8 ms-1. Pinal County storms showed slightly slower speed maxima at 5.4 to 12.4 ms-1. This Quarter displayed the highest wind speeds recorded, and that is largely attributed to the anomalous event on 17 August 2020. That storm traveled a greater distance horizontally and vertically than any other storm. The gravity-induced increase it experienced as it moved towards the lower central desert valleys accounts for the speed increase.

As with the top quarter of dust storms, Quarter 2 events show a strong signal from the Southwestern region but in this quarter of events, the Maricopa County events show activity in the south and Pinal storms begin to show activity in the Southeast. Some of these differences can again be explained by the position of the counties and the topography of the land. Pinal County is positioned slightly east and south of Maricopa County. Maricopa County has physical boundaries like the San Tan Mountains situated south of eastern Maricopa County, as well as the Picacho Mountains which are positioned at the southeastern edge of Pinal County. These features can block southeastern flows. The dust source region of these flows is located south of Picacho Peak in Pinal County. The Santa Cruz River is a tributary of the Gila River and is normally dry with visible soil erosion throughout its channel (Figure 3.7.B).

3.5.2.3 Quarter 3 dust storm events

Quarter 3 (dust concentrations ranked 25-50 percent of all events) shows a high concentration of events directly to the South and Southeast, and a reduction of events to the Southwest. The same thunderstorm and downburst activity driving dust over the Gila River in the Southwest are again at work here (Figure 3.9. A, B).

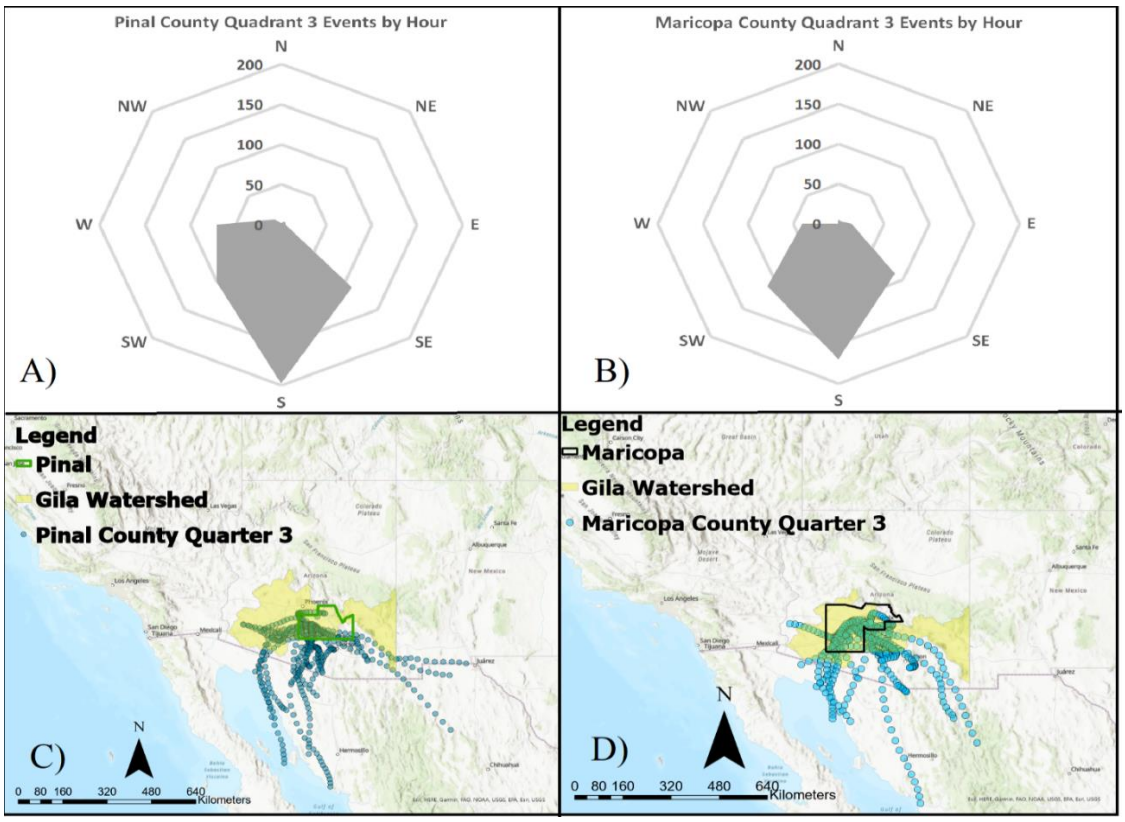

Figure 3.9. A) Pinal County Quarter 3 (dust concentrations ranked 25-50percent of all events) events wind rose plotted by hours of contact within each region B) Maricopa County Quarter 3 events wind rose plotted by hours of contact within each region C) Back-trajectory of all Quarter 3 dust storm events by latitude, longitude, and height for Maricopa County over a map of Southern Arizona highlighting the Gila River watershed and its tributaries. D) Back-trajectory of all Quarter 3 dust storm events by latitude, longitude, and height for Pinal County over a map of Southern Arizona highlighting the Gila River watershed and its tributaries

These events begin at or near the surface only rising the 500 m level by the time they reach their terminations. The highest starting surfaces for Maricopa County are 1850 m coming over the Pinal Mountains to the East. Pinal County dust storms demonstrated heights of 1359 m originating over central Mexico and coming in from the Southeast.

Maricopa County dust storms showed a maximum wind ranging from 4.5 to 11 ms-1. Pinal County showed slightly slower speed maxima ranging from 5 to 12 ms-1. Quarter 3 had the highest wind speeds recorded for Pinal County. This event (seen in Figure 3.9. C) occurred on 11 September 2011 and came from directly south passing over the Santa Rosa Wash into Pinal County. Its path is in the center of the map coming from the farthest south position.

Quarter 3 events originate from the South region for both counties. Along the south end of Pinal County and the far west edge of Maricopa County are a series dry washes that connect to the Santa Cruz River as it joined the Gila River. These dry washes run north from southern Arizona, such as the Vekol Wash (Figure 3.7. C). Surrounding the washes are a series of mountains like the Tabletop Mountains which funnel the wind through these dry channels. Not only do large NAM dust storms blow through the area but this area is also often an area of blowing dust during other times of the year.

3.5.2.4 Quarter 4 (lowest concentration) Events

For Quarter 4, the quarter of all dust storms with the lowest particulate concentration, the events are more broadly spread across all the southern areas (Figure 3.10. A, B). These events are the weakest storms with generally mild impact. These storms are more widely

dispersed with the three previous Quarters. They do not match the strength or concentration levels of the previous events as they do not originate from the major source regions identified for the other categories.

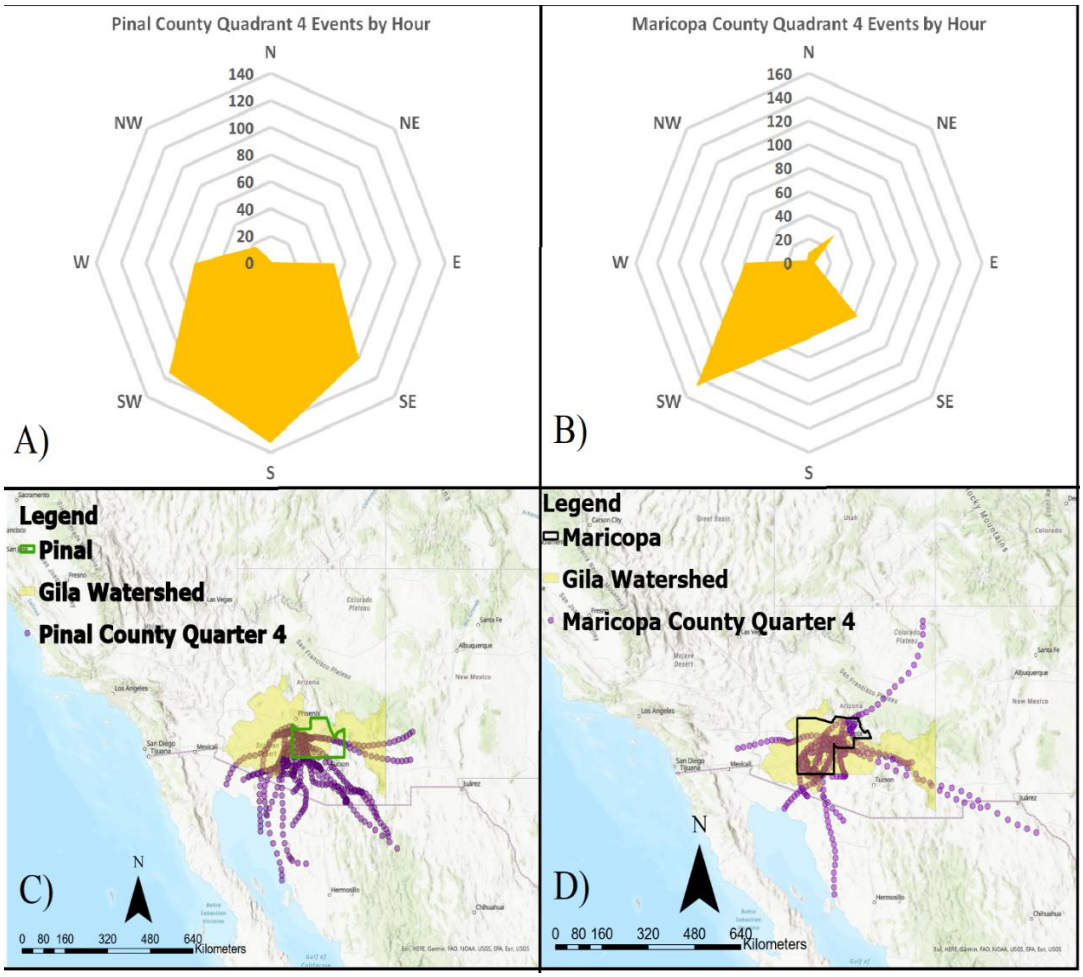

Figure 3.10. A) Pinal County Quarter 4 events wind rose plotted by hours of contact within each region B) Maricopa County Quarter 4 events wind rose plotted by hours of contact within each region C) Back-trajectory of all Quarter 4 dust storm events by latitude, longitude, and height for Maricopa County over a map of Southern Arizona highlighting the Gila River watershed and its tributaries. D) Back-trajectory of all Quarter 4 dust storm events by latitude, longitude, and height for Pinal County over a map of Southern Arizona highlighting the Gila River watershed and its tributaries

This more uniform distribution of directions for Quarter 4 dust storms allows for anomalies such as Maricopa County dust storm originating from the Colorado Plateau. This set of lowest concentration storms displayed surface heights ranging from at or near the surface to heights of 664-2084 m for Maricopa County and 605- 3649 m for Pinal County. The terrain prevents Maricopa County from getting as much activity from the southwest as Pinal County but that same positioning makes it less likely for Pinal County dust storm events to originate from the north and northeast. The highest wind speeds for Maricopa County ranged from 2.2 to 10.2 and 4.3 to 9.2 ms-1 for Pinal County. This weakest category of dust storms events demonstrated the smallest variation in wind speeds.

3.6. Conclusions

Dust storms are a major cause of Arizona weather fatalities (Mohebbi et al. 2019). They produce episodes of near-zero visibility leading to auto accidents (Mohebbi et al., 2019, Tong et al. 2023). This study has shown that such events tend to originate from south with ninety percent of the central Arizona dust storm events developing from southerly or near-southerly regions. The dust storms displaying the highest concentrations of particulate matter show a strong preference to originate from the southwest near the Gulf of California. This coincides with the development of a strong 500 hPa ridge to the east of the study area. The Quarter 1 (highest dust concentration) storms' back-trajectories display the overall lowest heights above the ground of the four Quarters. Given their predominant southwestern origin, these storms travel upslope along the Gila River and its

tributaries. These seasonally dry river beds are primary source regions for the largest dust storms in central Arizona.

Generation of weaker dust storms (Quarters 2-4) tend to have a wider spread with a greater shift to a southerly direction which indicates that the storms are traveling downslope through the many smaller washes and channels of the Santa Cruz River. As the maximum concentrations of dust lower, the overall height and direction of the storms drift east and higher.

Previous studies have highlighted how deadly these storms can be, and how important it is to understand and predict them (Tong et al. 2017, Tong et al. 2023, Achakulwisut et al. 2018). This paper highlights the spatial variations in central Arizona dust storms, showing the likeliest paths of the strongest events and assists in identifying aeolian dust origins.

Acknowledgments.

We thank all the members of the local scientific community who contributed vital information that made this paper possible, specifically Matthew Pace PhD, Meteorologist at Arizona Department of Environmental Quality ADEQ, Josh DeZeeuw, Air Quality Manager at Pinal County Air Quality, Eric Poole Jr., Monitoring Division Manager at Maricopa County Air Quality, and Ben Davis, Environmental Engineer at Air Quality Program Environmental Protection & Natural Resources Salt River Pima Maricopa Indian Community.

CHAPTER 4

TOPOGRAPHIC DUST SHIELDING AND FUNNELING: NORTH AMERICAN MONSOON CASE STUDIES FOR THE SONORAN DESERT, CENTRAL ARIZONA, USA

This chapter examines the summertime convective dust storms that form in the central Sonoran Desert and the local topographic features that effect the movement of dust storms in the region. A version of this paper will be published, titled as "Topographic Dust Shielding and Funneling: North American Monsoon Case Studies for the Sonoran Desert, Central Arizona, USA". Co-Authors on this paper are Robert C. Balling, Jr. Randall S. Cerveny. The data sources and software used in this analysis can be found in Appendix B.

Abstract

Dust storms are linked to large scale accidents and fatalities in the Central Sonoran Desert, specifically in the central Gila River Valley of the United States during the North American Monsoon. This study analyzes three cases where the underlying topography impacts large summertime dust storms and their movement. All three case examples demonstrate the shielding or, conversely, funneling effects associated the underlying terrain. The funneling between isolated mountain complexes, such as White Tank Mountains, the Sierra Estrella, the Sacaton Mountains, the San Tan Mountains, and the South Mountain Complex can combine to create substantially higher dust concentrations. Conversely, dust flow into these isolated mountain complexes can also lead to shielding, or blocking, of the dust such that area behind the topographic features

experiences less dust while the windward side of the barriers have accented dust concentrations. These dust storm/topography case studies provide a first opportunity to identify topographic influences on central Arizona dust storms.

4.1 Introduction

In the Sonoran Desert the North American Monsoon (NAM) dust storms are a continuing hazard. They are the third largest cause of weather-related fatalities in the Arizona, especially along the Interstate-10 corridor between Tucson and Phoenix (e.g., Mohebbi et al., 2019; Reid et al., 2015). In two separate instances in that same corridor there where three deaths reported from each and dozens of collisions also reported for each (December 22, 2009 and October 29, 2013) (Tong et al. 2023). These dust storm events are created by strong winds suspending sand or dust particulates over a large area. A dust storm warning, as defined by the National Weather Service, consists of atmospheric sand or dust with visibility by half a mile or less and wind speeds of 30 mph (13.4 ms^{-2}) or more (NWS 2009).

Studies have shown that the topography can greatly impact the flow and direction of dust storm movement, creating possible shielding effect that can reduce, or deflect dust (e.g., Lu et al. 2012; Mingari et al. 2017; Zhao-bin et al. 2019). If this topographic shielding can be verified through case examples, then there could be implications for heavily populated areas such as the central Sonoran Desert containing the Phoenix Metropolitan area. This could improve forecasts and allocation of resources, and ultimately save lives.

This study examines a set of three very strong dust storms that entered the Phoenix Metropolitan Area of eastern Maricopa and northern Pinal Counties in Arizona to identify if such shielding, or conversely the funneling of dust, by topography is evident.

4.2 Study Area and Past Research

The north-central region of the Sonoran Desert in the state of Arizona experiences many dust storm events during the North American Monsoon (NAM) from June 15 to September 30. Outflow from convective thunderstorms during the NAM time period typically produces most dust events affecting the region (Brazel and Nickling 1986). These events are characterized by strong winds and high concentration of particulate dust, leading to low atmospheric visibility. Official dust storm warnings issued by the National Weather Service are based on criteria of wind speeds at or exceeding 30 mph (13.4 ms^{-2}) and visibility of a half a mile or less (~0.8 km) (NWS, 2009).

Several previous studies (e.g., Maddox et al. 1995, Wallace et al. 1999, White et al., 2023) have examined how dust storms form and propagate in central Arizona. Specifically, such studies have identified that the shape of the Gila River Valley and the low elevation around the Phoenix metropolitan area create a drainage route that impacts storm movement and propagation Thunderstorms generally develop along the mountain ranges in the southern parts of the valley and travel north with gravity outflows. This movement through central Arizona as it encounters varying terrain (e.g., isolated mountain ranges) is a focal point for this paper.

Previous studies have examined aerosol movement through complex orographic terrain and the impacts on that movement. For example, researchers modeled the movement of smoke from wildfires through the Southern California terrain (Lu et al. 2012). They found that sharp changes in the topography can create areas of convergence or divergence of smoke at the surface. They suggested that the Sierra Nevada range could act as a large terrain block, in essence trapping smoke behind a wall. Additionally, the passes through the mountains can act as funnels that channel the smoke from the mountain valleys into the lowland areas of Los Angeles (Lu et al. 2012).

Similarly, in South America, numerical simulations have also tracked smoke, ash, and dust movement over the Fiambala' Basin in Northern Argentina (Mingari et al. 2017). That study specifically noted how the complex terrain of the Basin impeded the flow of atmospheric particulates through the Andes Mountains. Their findings indicated the difficulty in modeling low level transport over orographic barriers (Mingari et al. 2017).

In China, impact of the terrain on dust dispersion into the region was a focus of a study involving dust storms traveling from the Gobi Desert into Beijing (Zhao-bin et al. 2019). The study noted that, for a dust storm occurring on March 3, 2018, dust could not move directly into Beijing because the mountainous terrain blocked the flow. The topographic impediment forced the cold air mass containing the dust to flow downslope to the Yan Mountains where it then flowed into Beijing the following day (Zhao-bin et al. 2019). Similarly, a study of a dust storm on the Arabian Peninsula indicated that a dust storm occurring in March of 2012 was initially blocked by the mountainous terrain and then

channeled into smaller flows which then led dust plumes into the Red Sea (Vendrell et al. 2017).

Consequently, this study examines whether isolated elevated topography in central Arizona has demonstrated any effect on dust storms associated with the NAM. Dust storms during the NAM form under convective storm activity along the southern portion of the valley along the southern mountainous terrain (Maddox et al. 1995). Downbursts from the convective storms create cold pool outflows that move downslope creating dust storms (Wallace et al. 1999). To examine the possible impact of the terrain on dust storms, we have focused on three specific events; July 5, 2011, June 30, 2013, and August 17, 2020.

This paper focuses on the North-Central portion of the Sonoran Desert situated within the two counties of Maricopa and Pinal in the State of Arizona within the United States (Figure 1). This area is dotted with mountainous terrain, such as the South Mountain complex and San Tan Mountains. Some of these mountains reach over a thousand meters in height.

Data are collected from three major sources, the Storm Event Database produced by the National Oceanic and Atmospheric Administration (NOAA), the Hourly Particulate Matter in 10 micrometers (PM10) data provided by the Environmental Protection Agency (EPA), and the NEXRAD II radar data provided by NOAA. These sources show day, time, location, concentration, and movement of the north-central Sonoran dust storms during the summer monsoon period of June 15 to September 30. This time period follows

current NWS guidelines that give specific start/end dates to the National Oceanic and Atmospheric Administration. The Storm Event Database is managed by the National Centers for Environmental Information (NCEI) and provides classification data for dust storm events by county, including detailed spotter accounts (Murphy 2021).

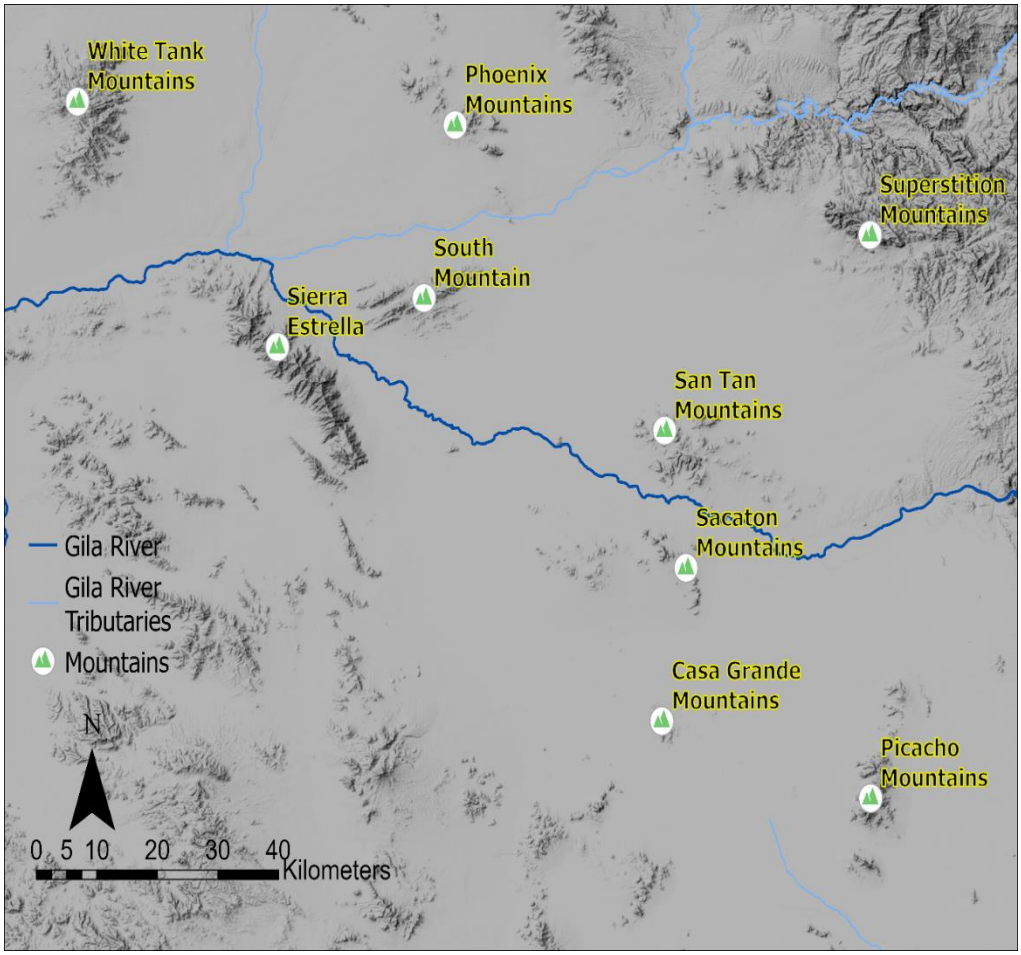

Figure 4.1. Gila River Valley (in dark blue), the Salt and Verde Rivers (in light blue) and surrounding mountains (in grey-shade): Casa Grande Mountains Highest Peak 716 m, Area ~13790 sq. m; Phoenix Mountains, Highest Peak 795 m, Area ~86580 sq. m; Picacho Mountains, Highest Peak 1373 m, Area ~166120 sq. m; Sacaton Mountains, Highest Peak 410 m, Area ~83480 sq. m; San Tan Mountains, Highest Peak 946 m, Area ~132830 sq. m.; Sierra Estrella, Highest Peak 1375 m, Area ~315120 sq. m; South Mountain, Highest Peak 820 m, Area ~110870 sq. m; White Tank Mountains, Highest Peak 1244 m, Area ~257350 sq. m.; Superstition Mountains, Highest Peak 1542, Area ~ 6.5 million sq. m.

The EPA hourly PM10 data are used together with the Storm Event data to select the specific case studies and provide necessary concentration data as well as wind speed and direction for those events. The EPA data are managed in Arizona by three different groups, the Arizona Department of Environmental Quality (ADEQ) at the state level. At the county level there are the Maricopa County Air Quality Department (MCAQD), and the Pinal County Air Quality Department (PCAQD). Each of these offices has to meet the EPA's hourly PM10 data standard helping to ensure a level of quality control over the data set (EPA 2007).

To supplement the EPA data, we accessed the Arizona Meteorological Network (AZMET) for wind speed and direction. The AZMET is a network of 27 meteorological stations positioned around Southern Arizona and managed by the University of Arizona's College of Agriculture and Life Sciences (Brown 1998). The site provides meteorological data including wind speed and direction, as well as other data such as soil moisture and temperature.

The final source of data for this analysis is the NEXRAD II radar data which are also managed by NOAA's NCEI. These data are retrieved through the NOAA Weather and Climate Toolkit which provides access to station data, satellite data, model data, and Radar data (Ansari et al. 2018). The toolkit allows access to NEXRAD level II data which can show the movement of a given storm cell and possibly highlight at the lowest levels dust movement in the atmosphere (Ansari et al. 2018).

4.3 Methods

The three specific dust storms selected for this study occurred within two Arizona counties in the northeastern region of the Sonoran Desert, specifically Maricopa and Pinal Counties. Basic information on the dust storms is provided in Table 1 with detailed information in subsequent sections of this paper.

Dust Storm Event GMT (LST)	Maximum PM10 Concentration (μm^{-3})	Maximum Wind Speed (ms^{-1})
6 July (5July), 2011	49377.1	15.08
1 July (30 June), 2013	13304.0	9.97
17 August (16 August), 2020	28161.0	8.80

Table 4.1 The three dust storm case examples with their maximum concentrations (μm^{-3}) and wind speeds (ms^{-1}).

While Table 1 gives the dust concentration and maximum winds recorded for the storms, the data do have some limitations. For example, in Arizona, the distribution of sites can be clustered in some areas, sparse or nonexistent in other locations. This creates potential gaps in the data. Therefore, the PM10 data are used in this study to build an interpolated field and to estimate the general movement of the dust outflow over time across the entire central Arizona region. These data are also used in conjunction with the radar NEXTEL II data.

Although radar detection of desert region dust and sand transport has had some success, (e.g., Bychkov et al. 2020), the most readily available radar data for north-central Sonoran Desert for the present study is based on a radar station that is located just South of the San Tan Mountains southeast of the Phoenix metropolitan area (Figure 1). This

location causes sections of the lowest scan of radar to be blocked by the mountainous terrain and thereby limits study of some dust shielding events.

To overcome these limitations, interpolation is required to interpret the impact of the terrain on a given dust storm event. Previous dust studies involving interpolation analysis have used an Inverse Distance Weighting (IDW) interpolation (e.g., Sajjadi et al. 2017). This method is a deterministic mathematical model that assumes closer values are more related than further values within its function:

$$ZZ_j = \frac{\sum_{i=1}^{n} W_i Z_i}{\sum_{i=1}^{n} W_i} \text{ and } W_i = \frac{1}{d_{ji}^{p}} \quad (4.1.)$$

where Z_j is the concentration at the j^{th} point, W_i is the weight of observed i^{th} point, d_{ji} is the distance from the i^{th} point to the j^{th} point, p is the power and n is total number of points (Sajjadi et al. 2017).

Sajjadi et al. (2017) selected the IDW method for their PM10 analyses as many of the station data points were clustered within an urban environment. However, a weakness for this IDW analysis is that it cannot interpolate above the highest given value within the system. This means if there were higher concentrations than were recorded at the specific stations, then the spatial analysis could become skewed.

Although satellite imagery has been a tool used to track dust movement and to help verify numerical model findings, it is not used in this study. Past dust storm research focused on Phoenix Arizona has noted that satellite imagery of dust storms for this region can be unreliable (Lei et al. 2016). This is because, as Lei and colleagues noted, the timing of

the satellite passing, effects of cloud cover, and intrinsic bias in the data can all affect the reliability of measurements.

4.4 Geography

The area of study for this research is the north-central region of the Sonoran Desert, specifically, the corridor between Phoenix and Tucson along the Central Gila River Valley where several of its tributaries converge (Figure 4.1). The cold pools that drive the dust storm activity form on the outer edges of this valley and flow downstream. This action drives the dust into this narrow corridor as it moves through along the river channels (Maddox et al. 1995, White et al. 2023). The dust moves into the valley and there it will encounter several low mountains, none that rise more than 1400 m off the valley floor. Since a dust storm is a primarily surface phenomenon, these sparely placed mountains may nevertheless impact its movement.

This means that the valley floor has several places where natural blockades and choke points exist which can impede, or shield, dust flow or act as a channel to force dust flow into a specific direction (Figure 4.2). These mountains are mostly in close proximity to the river channels that the dust most readily flows through creating natural barrier points that divert the path of storms. For instance, the gap between the Sacaton and San Tan mountains is ~7100 m with high peaks of 410 m at Sacaton Peak and 946 m at the San Tan Peak on either side of the Gila River. Northerly flowing cold pools will drift through this gap which can work as a shield blocking direct northerly flow and diverting it westward.

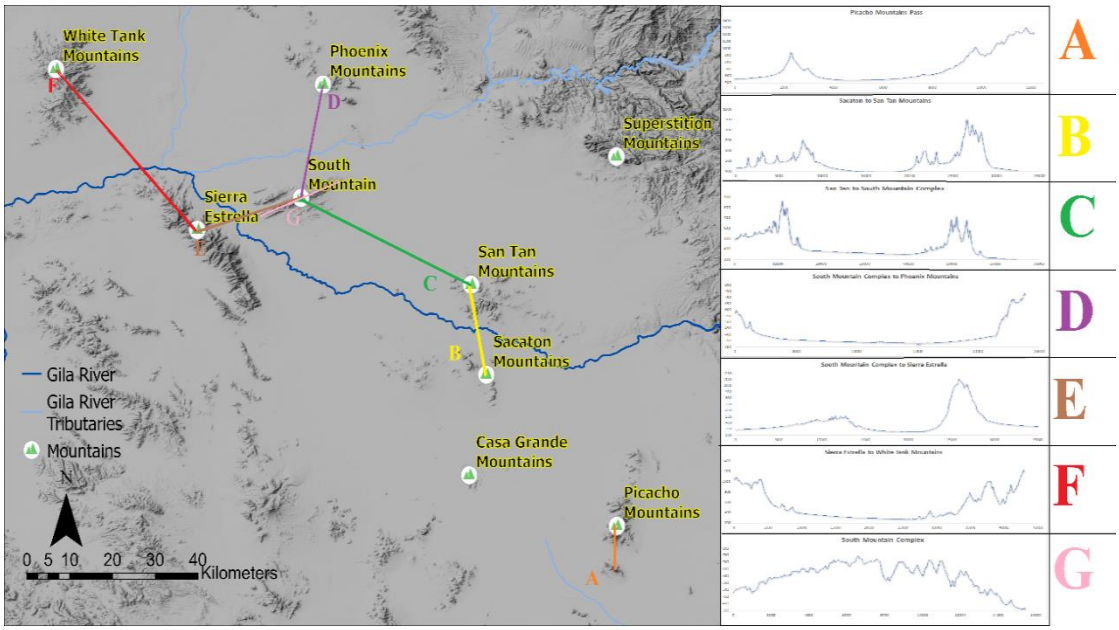

Figure 4.2. Topography of the north-central Sonoran Desert with cross-sectional profiles along specified mountain complexes. A) Picacho Peak Pass orange transect, ~4100 m B) Sacaton mts. to San Tan Mts., yellow transect, ~7160 m C) San Tan Mts. To South Mts., green transect, ~ 27700 m D) South Mts. to the Sierra Estrella, brown transect, ~8000 m E) South Mts. to Phoenix Mts., purple transect, ~20350 m F) Sierra Estrella to White Tank Mts., red transect, ~19000 m G) Telegraph Pass (South Mts. Complex) Pink transect~1000 m.

These narrow channels can also work as wind funnels that can intensify dust production. The area just north of Picacho Peak along the Interstate-10 freeway produces dust storms of near-zero visibility that can cause car accidents and fatalities (Tong et al. 2023). Looking at the topography, one can identify a narrow gap between the Picacho Mountains and the Picacho Peak of less than ~4100 m (Figure 4.2.).

4.4.1. 6 July, 2011 Event

A major dust storm (one of the largest dust storms to hit the Phoenix Metropolitan Area in recent decades) moved through the central Gila River Valley on July 6, 2011 from 01GMT to 06GMT (1800 LST – 2300 LST). IDW interpolation was performed for each hour of the storm on wind speed and direction, and on PM10 concentration levels to determine the path of the storm. As added confirmation, the lowest level cut (0.48) of the Base Reflectivity (BR) radar scan for each hour was collected and compared. This allowed for an hour-by-hour breakdown to illustrate the effect the topography can have on a surface level event like a dust storm.

At hour 01GMT (1800 LST), the IDW concentration field shows overall low-level dust concentrations, below the hourly threshold of 80 μm^{-3} per hour, except in the north-west corner between the Sierra Estrella and the White Tank Mountains (Figure 4.3.A). The IDW wind surface also shows convergence at that same point. These converging winds are occurring through the narrow pass between the White Tank Mountains and the Sierra Estrella. This would create a dust funneling effect similar to that seen for the smoke in the Sierra Nevada (Lu et al. 2012). The Base Reflectivity (BR) scan shows a moderate increase in the same region identified on Figure 3A, as well as showing high levels of reflectivity moving in from the south just beyond the range of the IDW fields (Figure 4A).

The second hour of the event, 02GMT (1900 LST), the BR image (Figure 4.4.B) begins to align with the IDW wind and concentration fields (Figure 4.3.B). A spike

occurs in the concentration (25,000 to 50,000 μm^{-3}) and wind speed levels increase (15 to 30 ms^{-1}) through the narrow gap between the Sacaton Mountains and the San Tan Mountains. As with the first hour, there are indications of the funneling effect as the storm moves through the narrow channel along the dry Gila River riverbed. The BR map also indicates high reflectivity at that same point in the mountains.

The third hour of the event, 03GMT (2000 LST), is the major thrust of the storm. The entire southern half of the IDW field is dominated by high concentrations of PM10 and high wind speeds (Figure 4.3.C). The northern half of the field, while still having high concentration and wind speed levels, are smaller by a factor of 10 (~50,000 μm^{-3} vs ~5,000 μm^{-3}). The BR radar image shows similar results, with higher levels of reflectivity throughout the southern half of the region (Figure 4.4.C). Variations in terrain contribute to this large discrepancy, the Sierra Estrella and the South Mountain Complex combine to create a substantial dust shield, blocking the dust from advancing northward. This is similar to the event described earlier in the Gobi Desert with the Yan Mountains diverting the flow of the dust flowing in the cold pool (Zhao-bin et al. 2019).

By the fourth hour 04GMT (2100 LST) the major dust concentrations of event has moved to the west outside of the IDW field (Figure 4.3.D) as the BR map as well (Figure 4.4.D). There is, however a small spike in the PM10 concentration (~1000 μm^{-3}) over the South Mountain Complex, which also aligns with north-pointing wind vectors on both the north and south sides of the mountain complex. In the middle of the South Mountain Complex is a small gap in the mountains called Telegraph Pass, which appears to be

acting as a dust funnel with the aligned wind fields creating a small spike in the dust concentration (Figure 4.3.D).

The final hour of the event 05 GMT (2200 LST) is mostly residual activity as the main storm has pressed on westward along the Gila River as shown by the BR radar image (Figure 4E). At this point the only remaining activity is to the west other than the remnant spike that was noted over the South Mountain Complex that has drifted northwest of the Gila River and along the west side of the Phoenix Mountains (Figure 4.3.E).

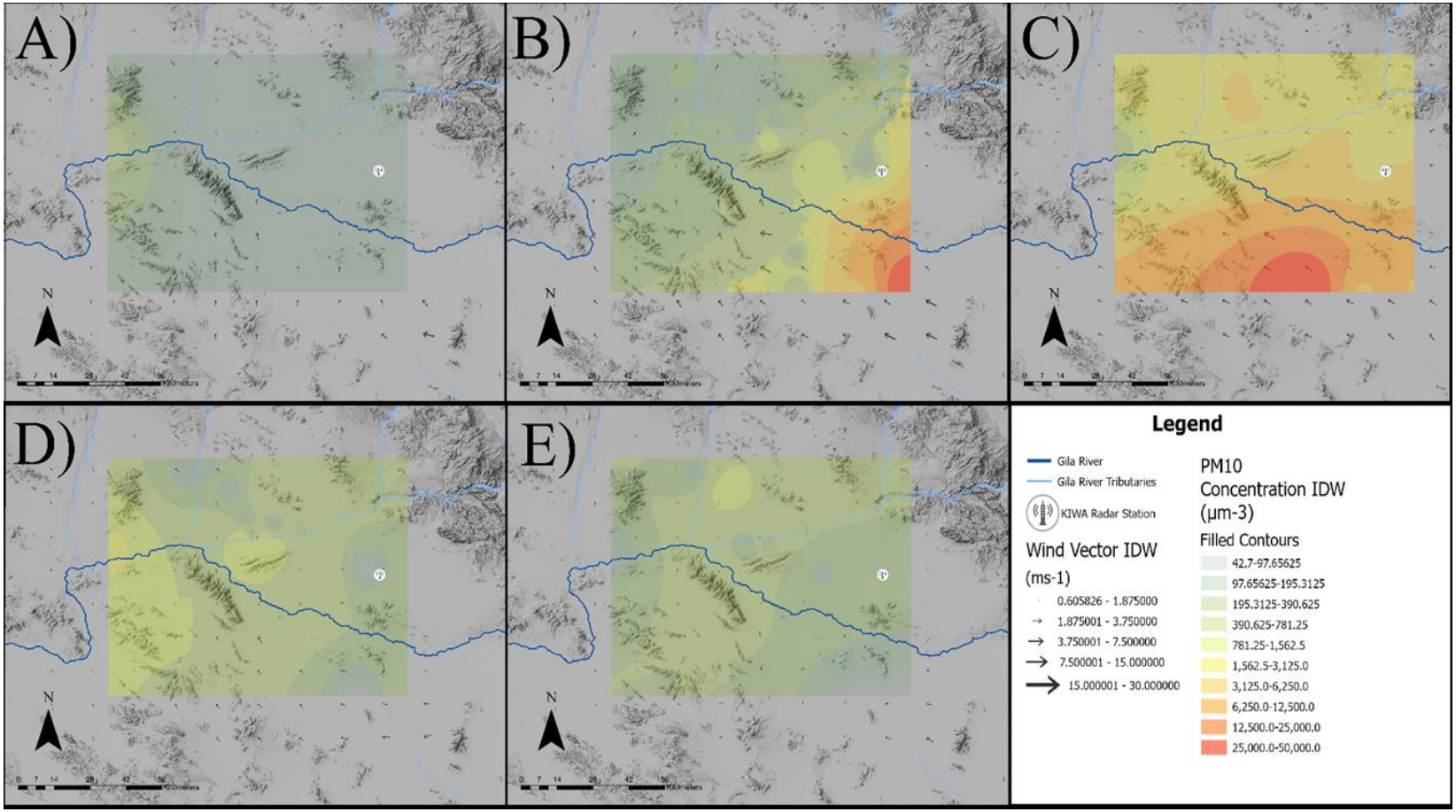

Figure 4.3. July 6, 2011 01 GMT to 05 GMT Gray Scale images of the Central Gila River Valley, dark blue line indicates Gila River, light blue lines indicate Gila River tributaries, black arrows indicate wind vectors, and the filled contours indicate PM10 field concentrations. A) July 6, 2011 01 GMT image of the PM10 and Wind Vector IDW fields. B) July 6, 2011 02 GMT image of the PM10 and Wind Vector IDW fields. C) July 6, 2011 03 GMT image of the PM10 and Wind Vector IDW fields. D) July 6, 2011 04 GMT image of the PM10 and Wind Vector IDW fields. E) July 6, 2011 05 GMT image of the PM10 and Wind Vector IDW fields. Last image Legend for A-E images.

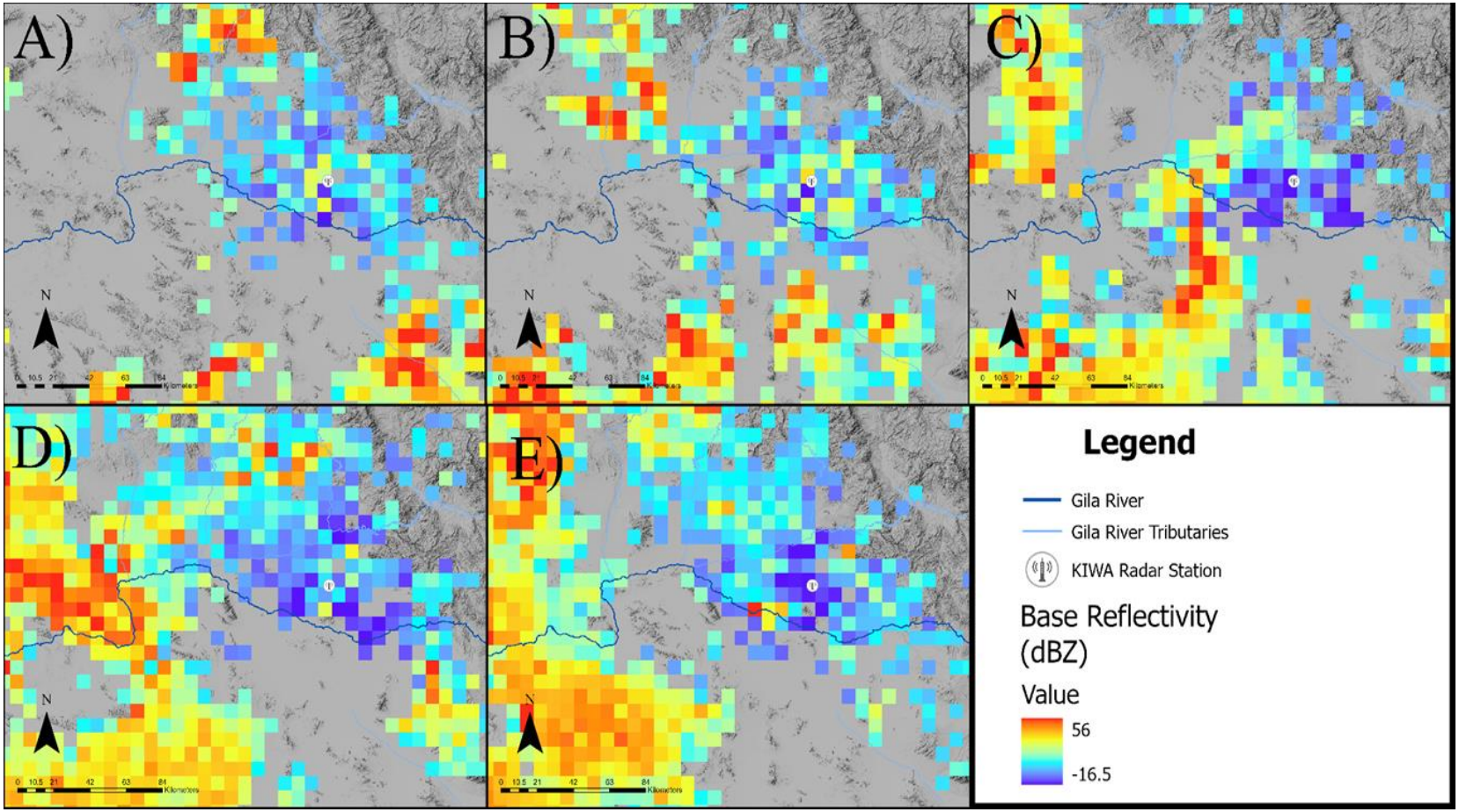

Figure 4.4. July 6, 2011 01 GMT to 05 GMT Gray Scale images of the Central Gila River Valley, dark blue line indicates Gila River, light blue lines indicate Gila River tributaries, Colored blocks indicate Base Reflectivity Radar images. A) July 6, 2011 01 GMT image of the Base Reflectivity. B) July 6, 2011 02 GMT image of the Base Reflectivity. C) July 6, 2011 03 GMT image of the Base Reflectivity. D) July 6, 2011 04 GMT image of the Base Reflectivity. E) July 6, 2011 05 GMT image of the Base Reflectivity. Last image Legend for A-E images.

4.4.2. 1 July, 2013 Event

A major dust storm moved through the Central Gila River Valley on July 1, 2013 from 04 GMT (2100 LST) to 07 GMT (0000 LST). As with the previous event, the path of the storm was plotted with IDW interpolation overlaid for each hour of the storm on wind speed and direction, and on PM10 concentration levels. The lowest level cut (0.48) of the Base Reflectivity (BR) radar scan for each hour was collected and compared to the concentration analysis. As with the first example, this hour-by-hour breakdown also illustrates the effect that the topography can have on a surface level event like a dust storm.

In contract to the previous case example's storm which moved from the southeast to the northwest, this storm has a more direct east-to-west flow. The first hour of the event at 04 GMT (2100 LST) shows peaks occurring in the southeast for both PM10 concentrations and wind speeds (Figure 5A). Additionally, a PM10 concentration spike is evident between the San Tan and Sacaton Mountains (Figure 4.5.A). The BR radar image shows a spike in reflectivity over that same point coinciding with the funneling activity (Figure 6A).

The concentrations associated with second hour of the event, 05 GMT (2200 LST), display an increase in activity. There is a large spike of ~13000 μm^{-3} centered around the open terrain to the west of the Sacaton Mountains (Figure 4.5.B). The BR radar image shows the same spike as the winds push the storm to the west (Figure 4.6.B). As with the previous case example, the highest concentration levels occur on the southern

half of the IDW field, which is the south side of the Gila River. The Sierra Estrella and South Mountain Complex hold the highest concentration levels in the south, effectively shielding the north side of the Gila River. There is also another visible spike in dust concentrations over central part of the South Mountain Complex right over the Telegraph Pass as the topography funnels the dust through the gap.

The third hour of the event (06 GMT, 2300 LST) is similar to the previous hour with most of the dust activity occurring on the southern side of the Gila River, but now there is a large spike in the PM10 concentrations between the South Mountain Complex and the Phoenix Mountain (Figure 4.5.C). This spike in the wind speed is created by the funneling effect created by airflow being pushed through the two mountain systems. In contrast, with the predominant easterly flow, the South Mountain Complex and the Sierra Estella act as a blocks or barriers that act to separate the larger spike in PM10 concentrations in the south from the north. Similarly, the BR radar image also displays the location and intensity of the dust as being on both sides of the Gila River (Figure 4.6.C).

For the last hour of the event (07 GMT, 0000 LST) most of the storm has pushed off to the northwest and west with the IDW concentration fields dropping precipitously in value from the previous hour (Figure 4.5.D). The BR radar image similarly shows a lower level of reflectivity within the IDW field, with the activity further south and west (Figure 4.6.D). The last remaining spike in PM10 and wind values is in the northwest corner of the map between the White Tank Mountains and the Sierra Estrella.

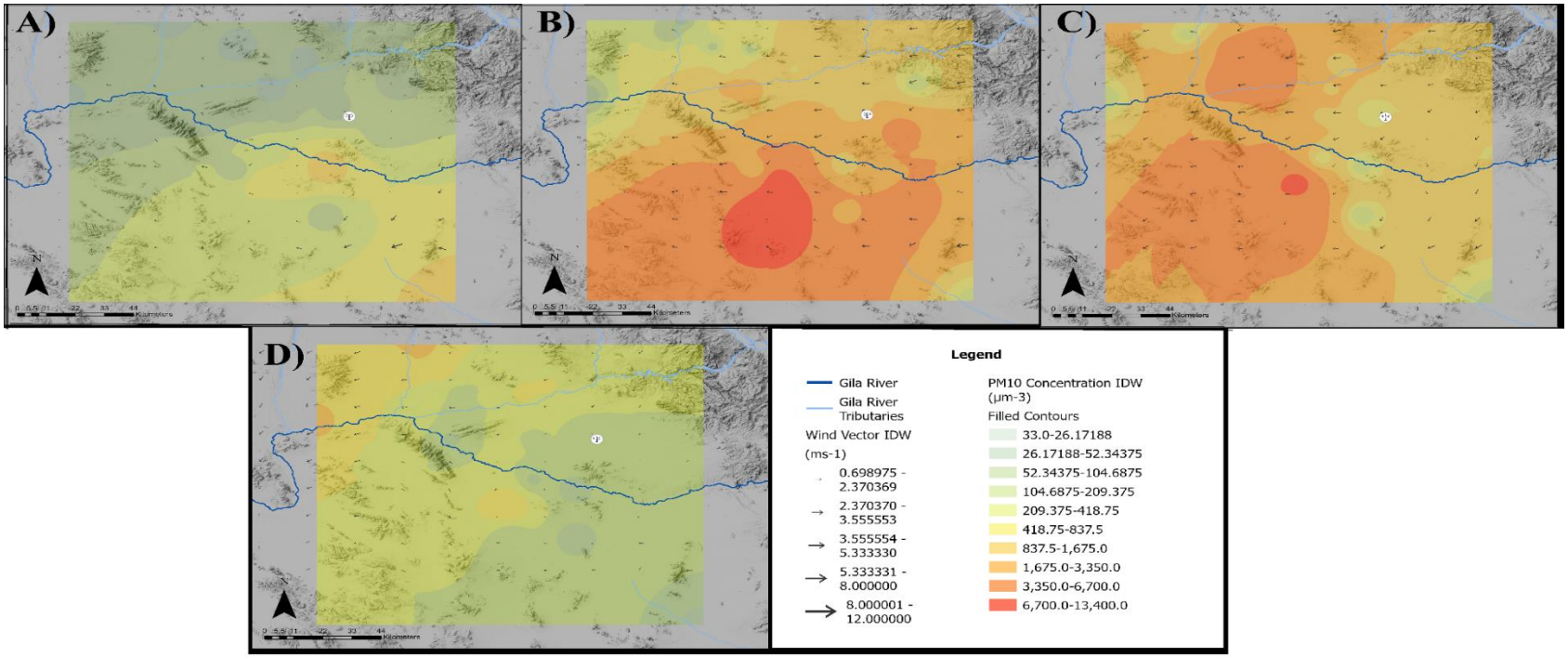

Figure 4.5. July 1, 2013 04 GMT to 07 GMT Gray Scale images of the Central Gila River Valley, dark blue line indicates Gila River, light blue lines indicate Gila River tributaries, black arrows indicate wind vectors, and the filled contours indicate PM10 field concentrations. A) July 1, 2013 04 GMT image of the PM10 and Wind Vector IDW fields. B) July 1, 2013 05 GMT image of the PM10 and Wind Vector IDW fields. C) July 1, 2011 06 GMT image of the PM10 and Wind Vector IDW fields. D) July 1, 2013 07 GMT image of the PM10 and Wind Vector IDW fields. Last image Legend for A-E images.

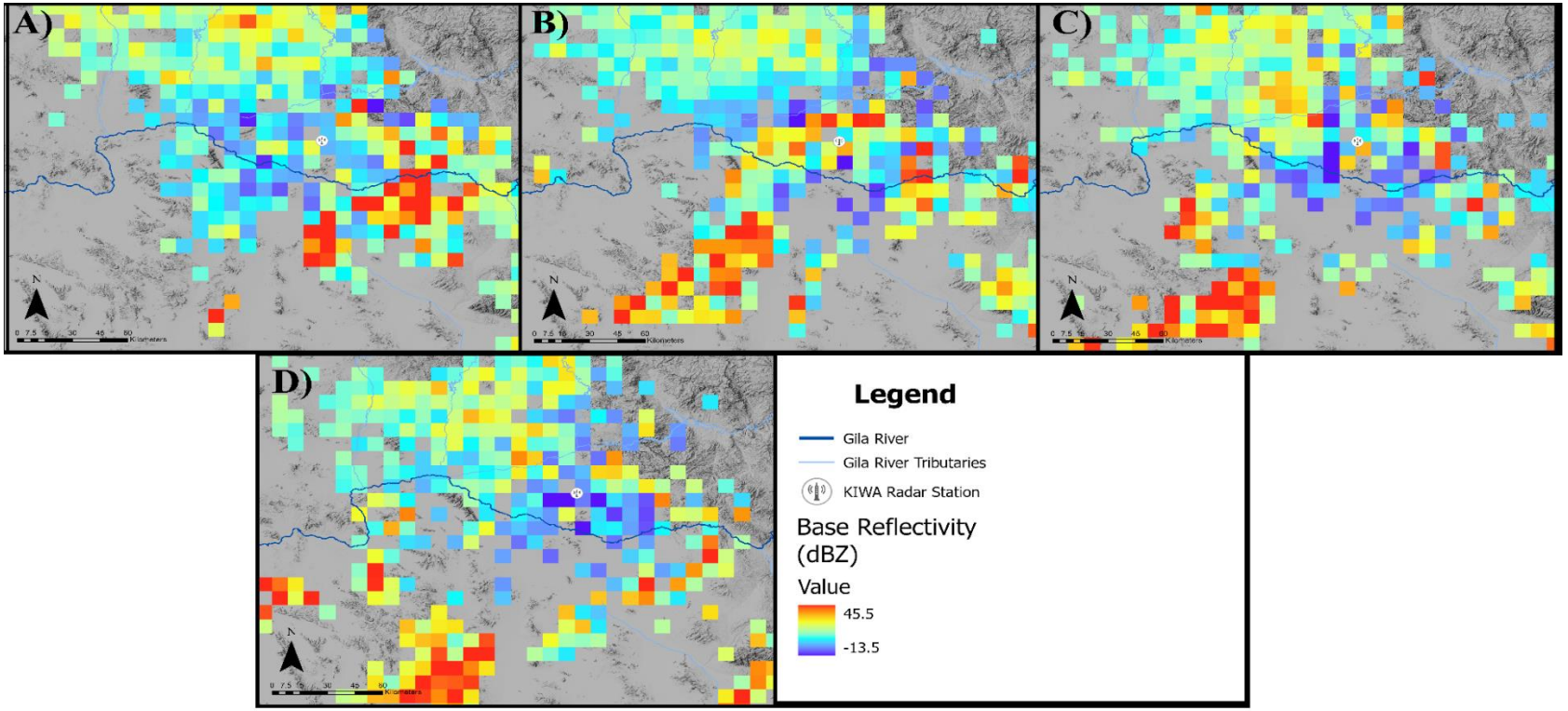

Figure 4.6. July 1, 2013 04 GMT to 75 GMT Gray Scale images of the Central Gila River Valley, dark blue line indicates Gila River, light blue lines indicate Gila River tributaries, Colored blocks indicate Base Reflectivity Radar images. A) July 1, 2013 04 GMT image of the Base Reflectivity. B) July 1, 2013 05 GMT image of the Base Reflectivity. C) July 1, 2013 06 GMT image of the Base Reflectivity. D) July 1, 2013 07 GMT image of the Base Reflectivity. Last image Legend for A-E images.

4.4.3. 17 August, 2020 Event

This case example of a dust storm occurring on August 16-17, 2020 (23 UTC-03 UTC, 1600-200 LST) is somewhat different than the previous two events because, rather than forming in the south, this dust storm formed in the north of the Phoenix Metropolitan Area along the Mogollon Rim. The Rim is a mountainous uplift fault that separates the Sonoran Desert from the Colorado Plateau in the extreme northeast corner of the central Gila River Valley. In the first hour of the event (23 GMT, 8-16-2020 23 GMT; 1600 LST), the storm winds are moving northward and there is only one area with any notable terrain-influenced activity. That is a small spike in the PM10 dust concentrations northeast of the Phoenix Mountain Complex as that mountain complex acts to shield dust movement southward (Figure 4.7.A). The BR radar image also indicates low level activity forming all along the Superstition Mountains (Figure 4.8.A).

The image of the second hour of the event (00 GMT, 1700 LST) displays the largest values for the PM10 dust concentration and wind speed (~28000 μm^{-3} and 15 ms^{-1}) (Figure 4.7.B). The winds have shifted from a southwesterly flow towards the mountains to a northeasterly wind direction, heading along the Salt River towards the southeast (Figure 4.7.B). The BR radar image indicates high reflectivity's in the same region as the PM10 dust concentration IDW and Wind fields (Figure 4.8.B). Similar to the previous storms' dust values, the highest dust concentrations of this storm are restricted to the south side of the Gila River. More precisely, the highest PM10 dust concentrations and wind speeds are situated the low-lying area between the Casa Grande

Mountains and the Picacho Mountains. The dust was funneled through inferring topography such that lower terrain between the two mountains displayed the high dust concentrations.

The third hour of this event (01 GMT, 1800 LST) has a smaller concentration spike in the PM10 values for the area between South Mountain Complex and the San Tan Mountains. In this case, the South Mountain Complex acts as a shield, or barrier, to dust flow along the north side of the Gila River Valley (Figure 4.7.C). While the BR radar images does not effectively show this spike, it could be that the timing gap in radar scans missed the rapid flow of dust or perhaps the dust was too low to register on the low-level radar scan. Regardless of the reason, in this instance, the radar scan did not replicate the shielding effect that is evident in the IDW analysis as clearly as previous examples (Figure 4.8.C).

The fourth hour (02 GMT, 1900 LST) produced another small concentration spike extending out on the north side of the Phoenix Metropolitan Area moving west to southwest as dust funneling occurs between the Phoenix Mountains and the South Mountain Complex. The topography pushed to the dust to into the Sierra Estella (Figure 4.7.D). The BR radar image shows this same area with high levels of reflectivity (Figure 4.8.D). In this instance the Sierra Estrella acts as a dust shield, blocking some of the dust as it moves into the next hour.

The last hour of this case example dust storm (03 GMT, 2000 LST) continued the movement of the small spike in the PM10 field over the Sierra Estrella with a decrease in

dust concentration from ~800 to 400 μm^{-3} from the previous hour (Figure 4.7.E) as the dust flow as inhibited by the mountains. Just as with the previous hour the BR radar image shows the same movement over the Estrella (Figure 4.8.E). As with the previous storms, there is an overall storm movement west to east, following the Gila River downslope movement and indicating gravity flow of the storm.

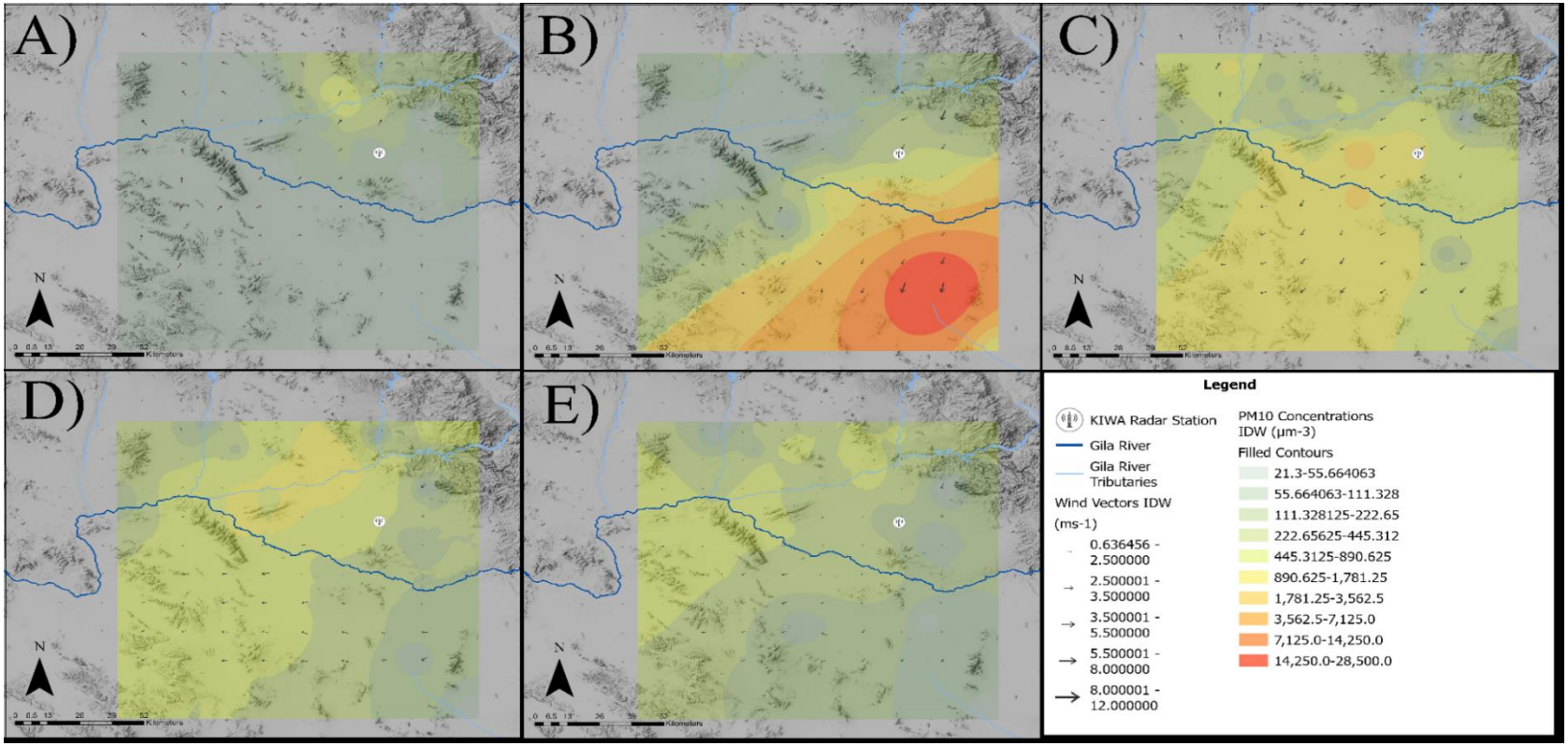

Figure 4.7. August 17, 2020 23 GMT to 03 GMT Gray Scale images of the Central Gila River Valley, dark blue line indicates Gila River, light blue lines indicate Gila River tributaries, black arrows indicate wind vectors, and the filled contours indicate PM10 field concentrations. A) August 16, 2020 23 GMT image of the PM10 and Wind Vector IDW fields. B) August 17, 2020 00 GMT image of the PM10 and Wind Vector IDW fields. C) August 17, 2020 01 GMT image of the PM10 and Wind Vector IDW fields. D) August 17, 2020 02 GMT image of the PM10 and Wind Vector IDW fields. E) August 17, 2020 03 GMT image of the PM10 and Wind Vector IDW fields. Last image Legend for A-E images.

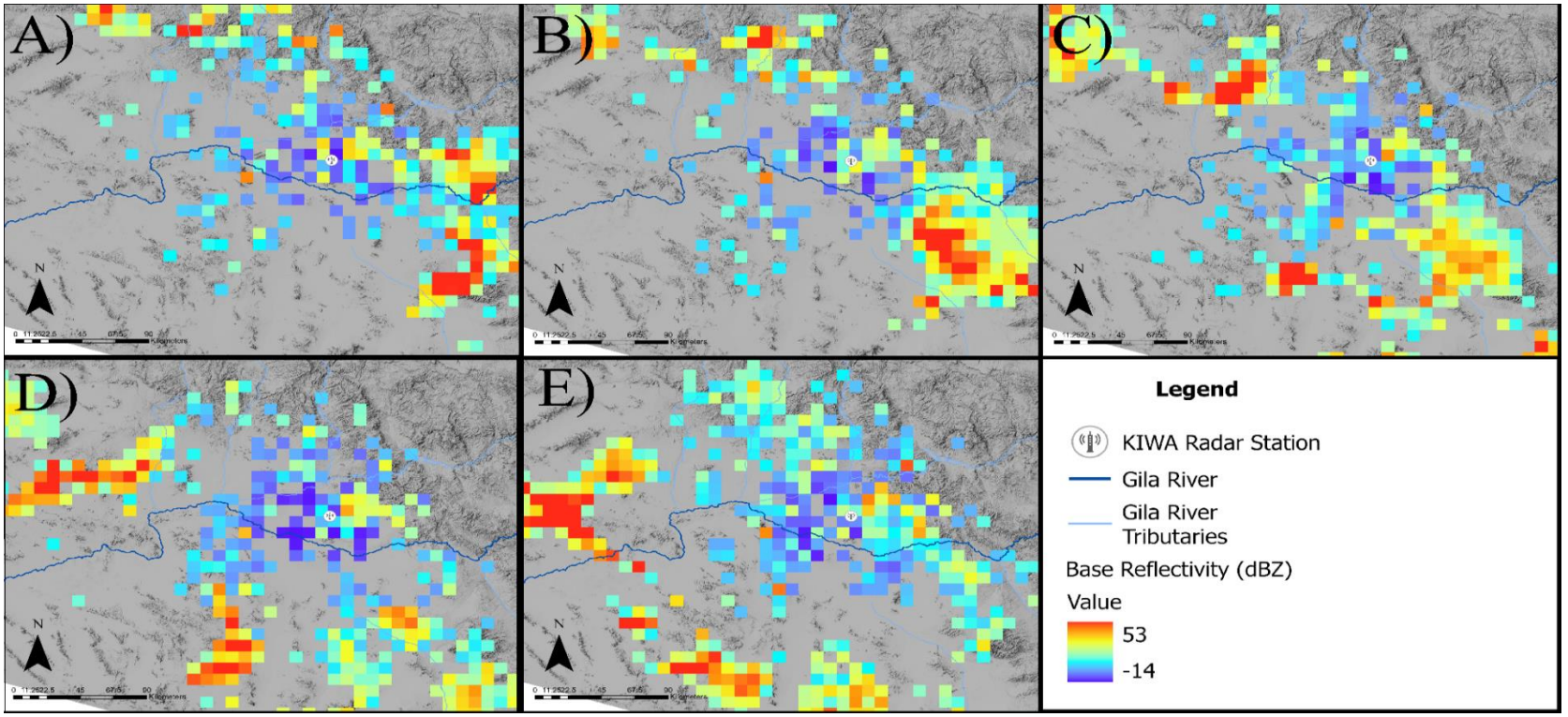

Figure 4.8. August 17, 2020 23 GMT to 03 GMT Gray Scale images of the Central Gila River Valley, dark blue line indicates Gila River, light blue lines indicate Gila River tributaries, Colored blocks indicate Base Reflectivity Radar images. A) August 16, 2020 23 GMT image of the Base Reflectivity. B) August 17, 2020 00 GMT image of the Base Reflectivity. C) August 17, 2020 01 GMT image of the Base Reflectivity. D) August 17, 2020 02 GMT image of the Base Reflectivity. E) August 17, 2020 03 GMT image of the Base Reflectivity. Last image Legend for A-E images.

4.5. Discussion and Conclusion

A recent study on dust storm fatalities show that dust storms are more deadly than previously believed, from 2007 to 2017 the fatality rate jumped from 10 deaths to 232 by adding the Fatality Analysis Reporting System (FARS) dataset (Tong et al. 2023). Many of those deaths occur in the central Gila River Valley near the topographic barriers discussed above. Each of the case studies presented have shown higher concentrations of PM10 dust due to the topographic barriers within the central Arizona region.

In the first case (July 6, 2011), the White Tank Mountains and the Sierra Estrella initially create a funneling effect as the IDW dust field shows a convergence of dust through the narrow pass between the two mountains. Later, during the storm, a similar spike in dust concentration and wind speeds occur through the narrow gap between the Sacaton Mountains and the San Tan Mountains. By the third hour of the storm, the Sierra Estrella and the South Mountain Complex combine to create a substantial dust shield, blocking the dust from advancing northward.

At the beginning of the second dust storm (1 July 2013), a funneling of surface dust is evident between the San Tan and Sacaton Mountains, creating a noticeable dust spike. This coincides with a BR radar image's spike in reflectivity over that same point. By the storm's second hour, the Sierra Estrella and South Mountain Complex effectively shield the north side of the Gila River, thereby holding the highest concentration levels in the south. A second noticeable spike in dust concentrations occurring in central part of the South Mountain Complex occurring through the Telegraph Pass as the topography funnels the dust through the gap. By the third hour, a large spike in the dust

concentrations between the South Mountain Complex and the Phoenix Mountain. This spike in the wind speed is created by the funneling effect created by airflow pushing dust through the two mountain systems. Towards the end of the storm, with the predominant easterly flow, the South Mountain Complex and the Sierra Estella act as a blocks or barriers that act to separate the larger spike in PM10 concentrations in the south from the north.

For the third case (August 17, 2020), wind funneling is evident in the early portions of the storm, as the highest dust concentrations are restricted to on the south side of the Gila River in the low-lying area between the Casa Grande Mountains and the Picacho Mountains. Dust is funneled through inferring topography leading to higher concentrations. By third hour of storm, a smaller dust is evident between the area between South Mountain Complex and the San Tan Mountains. In this case, the South Mountain Complex acts as a shield, or barrier, to dust flow along the north side of the Gila River Valley. Towards the end of the storm, dust funneling occurs between the Phoenix Mountains and the South Mountain Complex creates a small concentration spike extending out on the north side of the Phoenix Metropolitan Area.

Previous studies have shown that the Gila River and its tributaries are an important element to the formation and movement of dust storms in the Central Gila River Valley (White et al. 2023, Brazel and Nickling 1986). This paper extends that relationship to address the impact that the local isolated mountain topography can have on those dust storm events. Although the limited density of the available sensor network

inhibits the resolution of the IDW field, it provides a first opportunity to identify topographic influences on dust storms. Future research can model the topographic impact on dust storm using different starting locations to help identify areas where dust channeling or dust shielding may occur during any given event. These case studies also highlight the continued need for the development of a high-resolution network of dust sensors throughout the heavily populated central region of Arizona.

CHAPTER 5

5.1. Summary and Results

Dust storms have a variety of far-reaching human and economic impacts; from the spread of disease, raspatory and cardiovascular disruption, damage to property and crops, and even death. It is important to increase our understanding of this phenomenon, thus this dissertation posed this central question:

a) *Do dust storms have discreet geographic and temporal characteristics that can aid academic and operational analysis of these storms?*

Given that question, I broke this study into three separate questions:

b) *Is there a definable seasonal component to European dust "blood" rain events?*
c) *Is there a specific origin source for monsoon convective dust storms in the central Sonoran Desert region?*
d) *What topographic elements effect the movement of monsoon convective dust storm in the central Sonoran Desert region?*

To answer these subsequent questions, and ultimately the central question examining the geographic and temporal characteristics of dust storms, I undertook three separate studies covered over the course of the previous chapters within this dissertation.

5.2. Seasonality in European Red Dust/ "Blood" Rain Events (Case Study 1)

Colored rain events are a rare event for most of Europe, and previous studies had not closely examined the seasonal component on a continental scale. This study directly addresses that element by first building a dust rain archive of events across Europe, then

use three case studies to examine the synoptic conditions present for different regions of Europe. This analysis identifies some of the patterns associated with the seasonal dust rain events throughout Europe.

5.2.1. Dust Archive

To build the dust archive a total of 549 events across Europe where identified, using three primary sources: documented published papers, know events recorded by satellite data, and limited media accounts. While events have been recorded occurring year-round there is a seasonal aspect to their occurrences. The Iberian Peninsula has dust rain outbreaks throughout the year but with greatest frequency in the spring (MAM), the greatest frequency for all of Europe occurs in the spring as well. Western Europe has the fewest occurrences in the winter season (DJF). To explore these patterns three case studies for different regions were examined to determine the synoptic elements driving these events.

5.2.2. Case Studies

The first event was on June 22, 1988. The combination of upper air, TOMS AI, and HYSPLIT back-trajectory identifies the movement of dust from the Morocco/ Algeria region of northern Africa into Spain. Although this event is occurring in the summer, according to other studies on dust rain this is a common atmospheric pattern for the spring (Avila et al. 1997; Avila and Peñuelas 1999).

The second event was a dust rain storm occurring in Sweden on March 10, 1991. This analysis shows a large cutoff low was positioned over the Atlantic Ocean west of

France advecting dust from the same Morocco/ Algeria region of northern Africa to Sweden. Again, this fits the pattern of western Europe events occurring in the spring.

The third event was on April 18, 2005 in Turkey. This analysis shows a large cutoff low was positioned over northern Italy. Again, advecting dust from the same Algeria/ Libia region of northern Africa, this time to Turkey. This event shows the placement of a cutoff low drives the direction of the dust storms across Europe during the springtime.

5.2.3. Results

This study shows that while these colored rain events occur annually, the spring season has the highest concentration of dust rain events across Europe. These storms are driven by migratory Rossby waves combined with aerosol uplift from distinct North African source regions.

5.3. Trajectory Analysis of Central Sonoran Desert Dust Storms (Case Study 2)

Dust storms created during the NAM are a major concern for The Gila River Valley located in the Central Sonoran Desert. This study focuses on these dust storms that occur during the NAM from 2009 to 2022 using HYSPLIT back-trajectory analysis to determine the source region for these events. To accomplish this, data was extracted from a variety of sources and segregated by concentration levels.

5.3.1. Data

The raw data for this analysis was from two sources; NCDI and the EPA. To identify storms that occurred NCDI's Storm Event Database was used defining events within the given timeframe. These events where used to identify PM10 concentration levels provided by the EPA. This data identified two main counties effected by these dust storm events, Pinal and Maricopa. The events from each county were broken into four quarters based on PM10 concentration levels. Pinal and Maricopa where separated and examined separately with the central point of each county identified by their local airport (Casa Grande Regional and Sky Harbor respectively). Each county was divided into a circular region with a radius of ~644 km divided into eight distinct regions based on cardinal directions (W, NW, N, NE, E, SE, S, SW) with an area of ~96270 km^2. Each event was mapped over these regions using HYSPLIT back-trajectory for a 24-hour period before the event, and broken down by quarter.

5.3.2. Results

5.3.2.1. Synoptics

Almost every event for both counties comes from four directions based on the created regions; W, SW, S, and SE. To understand the synoptic forces driving these events a representative sample event for each direction was taken and compared using the NARR analysis of the 500 hPa geopotential height. For each event the position of the Subtropical High Pressure was closely related to the movement of the storm. Storms from the S and SE also had accompanying short wave troughs pushing through which can add to the upward movement of the storms.

5.3.2.2. Quarters

Quarter 1 dust storms for both counties had the largest number of events coming from the SW region along the Gila River. These storms generally start out at or near sea level by the Gulf of California moving along the Gila River across southern Arizona. Quarters 2-4 all show a strong signal towards the SW but begin to drift to the S and SE towards the Santa Cruz River and the smaller tributaries. As these storms drift E their overall starting height increases.

5.4. Topographic Dust Shielding and Funneling: North American Monsoon Case Studies for the Sonoran Desert, Central Arizona, USA (Case Study 3)

The third and final study of this dissertation focuses on dust storms created during the NAM in the Gila River Valley located in the Central Sonoran Desert. The local topography within the Gila River Valley can redirect the path of dust storms. To examine the possible effects of the local topography three case studies where conducted. This highlights some of those effects, including dust shielding and funneling.

5.4.1. Data and Methods

Just as the previous study used the NCDI Storm Event Database and the EPA PM10 concentrations, this study used that data to define three of the largest dust storm events from the 2009 to 2022 timeframe. That data was supplemented with wind speed

data from the EPA and with wind speed data from AZMET. I also collected radar data from the NCDI's Weather and Climate Toolkit NEXRAD level II data.

Three events where identified; July 5, 2011, June 30, 2013, and August 16, 2020. Then the features that could inhibit or enhance the movement of dust through the Gila River Valley where identified. There are a series of low-level stand-alone mountain complexes along the Gila River channel that can impede, or enhance dust flow.

Since it can be difficult to capture dust storms with satellite imagery in this region, another tool had to be employed to analyze the dust activity. To compensate for this, IDW interpolation of the PM10 concentrations and of the wind speeds was used.

5.4.2. Results

Depending on the path of the storm any of these mountains and gaps between them can either shield of funnel the dust as it flows through. In every instance the South Mountain Complex and the Sierra Estrella act as a shield at some point. The PM10 concentrations corroborate this. In every instance overall concentration levels are higher south of the South Mountain Complex and the Sierra Estrella.

5.4.2.1. 6 July, 2011

The first event shows a funneling effect through the White Tank Mountains and the Sierra Estrella with the IDW fields showing a convergence and spike of PM10 concentrations and wind. A similar spike occurs between the Sacaton and San Tan

Mountains. Meanwhile the South Mountain Complex and as the storm moves also the Sierra Estrella act as a dust shield that block the advancing storm.

5.4.2.2. 1 July, 2013

In the second case had several instances of dust funneling, between the San Tan and Sacaton Mountains, within the South Mountain Complex at the Telegraph Pass, and between the Phoenix Mountains and the South Mountain Complex. There where also instances of dust shielding; the Sierra Estrella and South Mountain Complex shield the north side of the Gila River and the Phoenix Metro area.

5.4.2.3. 17 August, 2020

The third case also had some instances of dust funneling; between the Casa Grande and Picacho Mountains, the South Mountain Complex and the San Tan Mountains, and between the South Mountain Complex and the Phoenix Mountains. More dust shielding occurs at the South Mountain Complex and the Phoenix Mountains.

5.5. Conclusions

Each chapter of this dissertation addressed three separate questions: Is there a definable seasonal component to European dust “blood” rain events? Is there a specific origin source for monsoon convective dust storms in the central Sonoran Desert region? And, what topographic elements effect the movement of monsoon convective dust storm in the central Sonoran Desert region? They were posed with the ultimate goal of examining one

overall question: Do dust storms have discreet geographic and temporal characteristics that can aid academic and operational analysis of these storms?

In each chapter, our knowledge of the geographic and temporal characteristics of dust storms was improved. First, I found that there is a definable seasonal component to European dust rain events, while they can occur at any time there is a trend for them to occur most frequently in the spring season due to migratory Rossby waves transporting dust from the Saharan Desert. Second, I discovered that there is there a specific origin source for monsoon convective dust storms in the central Sonoran Desert region. The largest events tend to originate from the southwest region, and the storms tend to drift to the south and east as they decrease in concentration. There is still an overall tendency for the storms to come from the southwest. Third and finally, I determined that there are topographic elements that effect the movement of monsoon convective dust storm in the central Sonoran Desert region. The stand-alone low elevation mountains throughout the Gila River Valley can affect the movement of dust storms by shielding or funneling dust as it passes through the region. Given these conclusions there are geographic (topography of the landscape and the synoptic conditions that create dust storms) and temporal characteristics (seasonal occurrences like NAM) that can aid academic and operational analysis of dust storms.

5.6. Implications/ Future Research

Each of the case studies in this dissertation address different elements of dust storms and therefore there are different implications for each sub study. There is however, a degree

of universality to them and future research should reflect those elements. The first case study highlights a relatively recent attempt to collect a database of dust rain events for Europe, continuing to build that database could offer more refinement showing hidden trends or of new changes due to climate change, and other factors like desertification. The same is true for dust storms in the Central Sonoran Desert, there have not been many studies cataloging dust storms in this region and the more data collected over time the more refined that dust archive can be at revealing trends and changes.

5.7 Fundamental Significance of this Dissertation

Aeolian dust transport can have a variety of consequences; heighten mortality rates (Tong et al. 2023), the spread of diseases (Goodie 2020), destruction of property and crops (Shepard 2016), or even the unusual and macabre display of blood rain. This dissertation has analyzed several of these elements, and defined of the trends that affect their movement and seasonal variations. These elements include the synoptic patterns that drive dust storms, the source regions of dust storms, and the ground level topography that can control their movement. Fundamentally, these findings can enhance our academic understanding of dust storm events as well as our operational understanding/ ability to forecast.

REFERENCES

Achakulwisut, P., Mickley, L. J., and Anenberg, S. C. 2018: Drought-sensitivity of fine dust in the US Southwest: Implications for air quality and public health under future climate change. *Envir. Res. Ltr.*, **13**(5), 054025.

Ansari, S., Del Greco, S., & Hankins, B. 2010, December: The weather and climate toolkit. In *AGU Fall Meeting Abstracts* 2010 pp. IN32A-06.

Ansari, S., Del Greco, S., Kearns, E., Brown, O., Wilkins, S., Ramamurthy, M., Weber, J., May, R., Sundwall, J., Layton, J. and Gold, A., 2018. Unlocking the potential of NEXRAD data through NOAA's Big Data Partnership. *Bull. Amer. Meteor. Soc*, *99*(**1**), 189-204.

Avila, A. and J. Peñuelas , 1999: Increasing frequency of Saharan rains over northeastern Spain and its ecological consequences. *The Sci. of The Total Enviro.*, **228**, 153-156.

Avila, A., I. Queralt-Mitjans and M. Alarcón, 1997: Mineralogical composition of African dust delivered by red rains over northeastern Spain. *J. Geophys. Res*., **102**. 21977-21996.

Brazel, A. J. and W. G. Nickling 1986: The relationship of weather types to dust storm generation in Arizona (1965-1980). *Intl. J. of Climatol.*, **6**, 255-275.

Burt, S., 1991: Falls of Dust Rain Within the British Isles. *Weather*, **46**, 347-352.

Bychkov, D., Ivanov, V., Matveyev, A., Tsymbal, V., & Yatsevich, S. 2020: Space-borne radar observation of near-surface wind effect on anomalously highly-directional backscattering of radio waves from Aeolian processes of sand and dust transporting in desert regions. *Ukrainian J. of Rem. Sens.*, (**24**), 4-8.

Carlaw, L. B., Ariel E. C., and Jaret W. R. 2017: Synoptic and mesoscale environment of convection during the North American monsoon across central and southern Arizona. *Wea. Forecasting* **32**(2), 361-375.

Cerveny, R. S., 2006: Freaks of the Storm, Thunder's Mouth Press (Avalon Publishing Group), New York, pp.371

Cook, E. R., Seager R., Cane, M. A., and Stahle, D. W., 2007: North American drought: Reconstructions, causes, and consequences. *Earth-Sci Rev.*, **81**, 93-134.

Coz, E., F. J. Gómez-Moreno, M. Pujadas, G. S. Casuccio, T. L. Lersch and B. Artíñano, 2009: Individual particle characteristics of North African dust under different long-range transport scenarios. *Atmo. Enviro*., ***43***, 1850-1863.

Dessens, J., 1990: Frequent Saharan dust outbreaks north of the Pyrenees: a sign of climatic change. *Weather*, ***45***, 327-333.

Draxler, R. R, 1999: HYSPLIT4 user's guide. NOAA Tech. Memo. ed. N. A. R. Laboratory. Silver Springs, MD: NOAA Air Resources Laboratory.

Draxler, R. R., and G.D. Hess, 1997: Description of the HYSPLIT_4 modeling system. NOAA

Tech. Memo. ed. N. A. R. Laboratory, 24. Silver Springs, MD: NOAA Air Resources Laboratory, 1998: An overview of the HYSPLIT_4 modeling system of trajectories, dispersion, and deposition. *Australian Meteor. Mag.*, **47**, 295-308.

Draxler, R. R. and G.D. Rolph, 2011: HYSPLIT (HYbrid Single-Particle Lagrangian Integrated Trajectory) Model access via NOAA ARL READY Website(http://ready.arl.noaa.gov/HYSPLIT.php) Silver Springs, MD: NOAA Air Resources Laboratory.

EPA, 2007: The Plain English Guide to the Clean Air Act. *Office of Air Quality Planning and Standards Research* Triangle Park, NC. Publication No. EPA-456/K-07-001

Franzén, L. G., J. O. Mattsson, M. Ulrik, T. Nihlén & A. Rapp, 1994: Yellow Snow over the Alps and Subarctic from Dust Storm in Africa, March 1991. *Ambio*, **23**, 233-235.

Gillette, D. A. and Hanson, K. J. 1989: Spatial and Temporal Variability of Dust Production Caused by Wind Erosion in the United States. *J. Geophys. Res*., **94**, 2197-2206.

Joshi, J. R. 2021: Quantifying the impact of cropland wind erosion on air quality: A high-resolution modeling case study of an Arizona dust storm. *Atmos.c Envir.*, **263**, 118658.

Kalnay, E., M. Kanamitsu, R. Kistler, W. Collins, D. Deaven, L. Gandin, M. Iredell, S. Saha, G. White, J. Woollen, Y. Zhu, A. Leetmaa, R. Reynolds, M. Chelliah, W. Ebisuzaki, W. Higgins, J. Janowiak, K. C. Mo, C. Ropelewski, J. Wang, R. Jenne & D. Joseph, 1996: The NCEP/NCAR 40-Year Reanalysis Project. *Bull. Amer. Meteor. Soc*, **77**, 437-471.

Lei, H., Wang, J. X., Tong, D. Q., & Lee, P. 2016: Merged dust climatology in Phoenix, Arizona based on satellite and station data. Climate Dynamics, **47**, 2785-2799.

Lu, W., Zhong, S., Charney, J. J., Bian, X., & Liu, S. 2012: WRF simulation over complex terrain during a southern California wildfire event. Journal of Geophysical Research: Atmospheres, 117(D5). https://doi.org/10.1029/2011JD017004

Maddox, R. A., McCollum, D. M., and Howard, K. W. 1995: Large-scale patterns associated with severe summertime thunderstorms over central Arizona. *Wea. Forecasting*, **10**, 763-778.

Maddox, R. A., Canova, F., and Hoxit, L. R. 1980: Meteorological characteristics of flash flood events over the western United States. *Mon. Wea. Rev.*, **108**(11), 1866-1877.

McPeters, R.D, Bjartia, P.K., Krueger, A.J., Herman J.R., Schlesinger, B.M., Wellemey, C.G., Sefor, C.J., Jaross, G., Taylor, S.L., Swissler, T., Torres, O., Labow, G., Bylerly, W., and Cebula, R.P.,1996: Nimbus–7 Total Ozone Mapping Spectrometer (TOMS) Data Products User's Guide. NASA Reference Publication. NASA, Lanham, MD p.18

Mohebbi, A., Green, G.T., Akbariyeh, S., Yu, F., Russo, B.J. and Smaglik, E.J., 2019: Development of dust storm modeling for use in freeway safety and operations management: an Arizona case study. *Trans. Res. Rec.*, **2673**(5), 175-187.

Moulin, C., and Chiapello, I, 2004: Evidence of the control of summer atmospheric transport of African dust over the Atlantic by Sahel sources from TOMS satellites (1979–2000). *Geophys. Res. Lett*., **31**(2).

Murphy, J. D. July 26, 2021: Storm Data Preparation (National Weather Service Instruction 10-1605). Retrieved on March 13, 2023 from http://www.nws.noaa.gov/directives/sym/pd01016005curr.pdf.

NWS, 2009: National Weather Service Glossary. Silver Spring, MD: US Dept of Commerce National Oceanic and Atmospheric Administration National Weather Service Flagstaff Weather Forecast Office.

NOAA, 2023a: Backward trajectory ending at 0300 UTC 06 JUL 11. NOAA Air Resources Laboratory Transport & Dispersion Modeling HYSPLIT. Retrieved March 20, 2023, from https://www.ready.noaa.gov/hypub-bin/trajresults.pl?jobidno=193479

NOAA, 2023b: April 5: JUL 05 12Z, 2011 NARR Daily Individual Obs. 500.0 mb Geopotential Height. NOAA Air Physical Sciences Laboratory NCEP North American Regional Reanalysis (NARR). Retrieved March 20, 2023, from https://psl.noaa.gov/mddb2/makePlot.html?variableID=116113

Okin, G. S., and Reheis, M. C., 2002: An ENSO predictor of dust emission in the southwestern United States. *Geophys. Res. Lett*., **29**, 1332.

Özsoy, T. and S. Örnektekin , 2009: Trace elements in urban and suburban rainfall, Mersin, *Northeastern Mediterranean. Atmos. Research*, **94**, 203-219.

Reheis, M. C. 2006: A 16-year record of eolian dust in Southern Nevada and California, USA: Controls on dust generation and accumulation. *J. of Arid Enviro.*, **67**, 487-520.

Reid, S. B., MacDonald, C. P., Alrick, D. M., Veneziano, D. A., Koon, L., Pryor, D., and Ginn, D. 2015: *Comm. Plan for Windblown Dust* (No. FHWA-AZ-15-723). Arizona. Dept. of Transportation.

Reynolds, R., Belnap, J., Reheis, M., Lamothe, P. and Luiszer, F., 2001: Aeolian dust in Colorado Plateau soils: nutrient inputs and recent change in source. *Proceedings of the Nat'l Acad. of Sci.*, **98**(13), pp.7123-7127.

Reynolds, R., Neff, J., Reheis, M. and Lamothe, P., 2006: Atmospheric dust in modern soil on aeolian sandstone, Colorado Plateau (USA): Variation with landscape position and contribution to potential plant nutrients. *Geoderma*, **130**(1-2), pp.108-123.

Rolph, G. D., 2011: Real-time Environmental Applications and Display sYstem (READY) Website (http://ready.arl.noaa.gov). Silver Spring, MD: NOAA Air Resources Laboratory.

Rolph, G., Stein, A., and Stunder, B. 2017: Real-time environmental applications and display system: READY. *Envir. Mod. & Software*, ***95***, 210-228.Santos, R. P. D. (2016). Some comments on the reliability of NOAA's Storm Events Database. arXiv preprint arXiv:1606.06973.

Sajjadi, S.A., Zolfaghari, G., Adab, H., Allahabadi, A. and Delsouz, M., 2017: Measurement and modeling of particulate matter concentrations: Applying spatial analysis and regression techniques to assess air quality. *MethodsX*, **4**, 372-390.

Santos, R. P. D. 2016: Some comments on the reliability of NOAA's Storm Events Database. *arXiv preprint arXiv:1606.06973*.

Stein, A. F., Draxler, R. R., Rolph, G. D., Stunder, B. J., Cohen, M. D., and Ngan, F. 2015: NOAA's HYSPLIT atmospheric transport and dispersion modeling system. *Bull. Amer. Meteor. Soc.*, **96**(12), 2059-2077.

Tong, D. Q., Wang, J. X., Gill, T. E., Lei, H., and Wang, B. 2017: Intensified dust storm activity and Valley fever infection in the southwestern United States. *Geophys. Res. Lett.*, **44**(9), 4304-4312.

Tong, D., Feng, I., Gill, T. E., Schepanski, K., and Wang, J. 2023: How many people were killed by windblown dust events in the United States. *Bull. Amer. Meteor. Soc.*, **104**(5), E1067-E1084.

Vendrell, L., Basart, S., & Baldasano Recio, J. M. (2017). Effect of terrain relief on dust transport over complex terrains in West Asia. In *Book of Abstracts* (May, 2017, pp. 64-65). *Barcelona Supercomputing Center*. http://hdl.handle.net/2117/107992

Wallace, C.E., Maddox, R.A. and Howard, K.W., 1999: Summertime convective storm environments in central Arizona: Local observations. *Wea. Forecasting*, **14**(6), pp.994-1006.

White, J. R., Cerveny, R. S., and Balling, R. C. 2012: Seasonality in European red dust/ "blood" rain events. *Bull. Amer. Meteor. Soc.*, **93**(4), 471-476.

APPENDIX A

DATASETS AND SOFTWARE ACCESSED FOR CHAPTER 3

TRAJECTORY ANALYSIS OF CENTRAL SONORAN DESERT DUST STORMS

A.1. Datasets

EPA 2023: Tables of Hourly Data PM10. EPA Air Data Pre-Generated Data Files. Subset used: 2009 – 2023, Retrieved 21 March 2023, from https://aqs.epa.gov/aqsweb/airdata/download_files.html#AQI

NOAA/ Air Resources Laboratory 2023: Backward Trajectory Calculations. NOAA Air Resources Laboratory Transport & Dispersion Modeling HYSPLIT. Data accessed from15 June 2009- 30 September 2022, Retrieved 20 March, 2023, from https://www.ready.noaa.gov/hypub-bin/trajasrc.pl

NOAA/ NARR 2023: NARR Daily Individual Obs. 500.0 mb Geopotential Height. NOAA Air Physical Sciences Laboratory NCEP North American Regional Reanalysis (NARR). Data accessed from15 June 2009- 30 September 2022, Retrieved March 20, 2023, from https://psl.noaa.gov/data/gridded/data.narr.html

NOAA/NCEI 2023: NOAA/ NCEI Storm Events Database. Data accessed for Dust Storm search for Maricopa and Pinal Counties 15 June 2009- 30 September 2022. Retrieved March 18, 2023 from https://www.ncdc.noaa.gov/stormevents/choosedates.jsp?statefips=4%2CARIZONA

A.2. Software

ESRI 2023. ArcGIS PRO Desktop: Release 3:1.2. Redlands, CA: Environmental Systems Research Institute. https://www.esri.com/en-us/arcgis/products/arcgis-pro/resources

APPENDIX B

DATASETS AND SOFTWARE ACCESSED FOR CHAPTER 4

TOPOGRAPHIC DUST SHIELDING AND FUNNELING: NORTH AMERICAN MONSOON CASE STUDIES FOR THE SONORAN DESERT, CENTRAL ARIZONA, USA

B.1. Datasets

AZMET 2023: The Arizona Meteorological Network Archive Files 2011- 2020, Retrieved December 20, 2023, from https://ag.arizona.edu/azmet/az-data.htm

EPA 2023: Tables of Hourly Data PM10. EPA Air Data Pre-Generated Data Files. Subset used: 2011 – 2020, Retrieved 21 March 2023, from https://aqs.epa.gov/aqsweb/airdata/download_files.html#AQI

NOAA/ NCEI 2023: NOAA/ NCEI Weather and Climate Toolkit (WCT). NOAA Next Generation Weather Radar (NEXRAD II) . Data accessed from15 June 2011- 30 September 2020, Retrieved December 20, 2023, from https://www.ncei.noaa.gov/products/radar/next-generation-weather-radar

NOAA/NCEI 2023: NOAA/ NCEI Storm Events Database. Data accessed for Dust Storm search for Maricopa and Pinal Counties 15 June 2011- 30 September 2020. Retrieved March 18, 2023 from https://www.ncdc.noaa.gov/stormevents/choosedates.jsp?statefips=4%2CARIZONA

B.2. Software

ESRI 2023. ArcGIS PRO Desktop: Release 3:1.2. Redlands, CA: Environmental Systems Research Institute. https://www.esri.com/en-us/arcgis/products/arcgis-pro/resources